

Chemical enrichment in LINERs from MaNGA. I. Tracing Oxygen and Nitrogen Nuclear Abundances in LINERs with Varied Ionizing Sources

Borja Pérez-Díaz¹, Enrique Pérez-Montero¹, Igor A. Zinchenko^{2,3}, and José M. Vílchez¹

¹ Instituto de Astrofísica de Andalucía (IAA-CSIC), Glorieta de la Astronomía s/n, 18008 Granada, Spain
e-mail: bperez@iaa.es

² Faculty of Physics, Ludwig-Maximilians-Universität, Scheinerstr. 1, 81679 Munich, Germany

³ Main Astronomical Observatory, National Academy of Sciences of Ukraine, 27 Akad. Zabolotnoho St 03680 Kyiv, Ukraine

Received MONTH DAY, YEAR; accepted MONTH DAY, YEAR

ABSTRACT

Context. The chemical enrichment in low-ionization nuclear emission-line regions (LINERs) is still an issue with spatial resolution spectroscopic data due to the lack of studies and the uncertainties in the nature of their ionizing source, despite being the most abundant type of active galaxies in the nearby Universe.

Aims. Considering different scenarios for the ionizing source (hot old stellar populations, active galactic nuclei (AGN) or inefficient accretion disks), we analyze the implications of these assumptions to constrain the chemical content of the gas-phase interstellar medium (ISM).

Methods. We used a sample of 105 galaxies from Mapping Nearby Galaxies at Apache Point Observatory (MaNGA) survey, whose nuclear central spaxels show LINER-like emission. For each scenario considered, we built a grid of photoionization models (4928 models for each considered ionizing source) which are later used in the open-source code HII-CHI-MISTRY, allowing us to estimate chemical abundance ratios such as $12+\log(\text{O}/\text{H})$ or $\log(\text{N}/\text{O})$ and constrain the ionization parameter that characterize the ionized ISM in those galaxies.

Results. We obtain that oxygen abundances in the nuclear region of LINER-like galaxies spread over a wide range $8.08 < 12+\log(\text{O}/\text{H}) < 8.89$, with a median solar value (in agreement with previous studies) if AGN models are considered. Nevertheless, the derived nitrogen-to-oxygen ratio is much less unaffected by the assumptions on the ionizing source, and point towards suprasolar values ($\log(\text{N}/\text{O}) = -0.69$). By comparing the different analyzed scenarios, we show that if hot old stellar populations were responsible of the ionization of the ISM a complex picture (such as outflows and/or inflows scaling with galaxy chemical abundance) would be needed to explain the chemical enrichment history, whereas the assumption of AGN activity is compatible with the standard scenario found in most galaxies.

Key words. Galaxies: ISM – Galaxies: abundances – Galaxies: active – Galaxies: nuclei

1. Introduction

Among the different approaches for analyzing the evolution of galaxies, the metal content of the interstellar medium (ISM) is a very important constrain. While Big Bang Nucleosynthesis allows us to explain the majority of hydrogen (H), helium (He), lithium (Li) and deuterium (D) present in the ISM (Cyburt et al. 2016), nearly all the rest of elements are produced by means of the different star formation processes that govern the evolution of galaxies (e.g. Kobayashi et al. 2020; Duarte Puertas et al. 2022), ultimately shaped by other processes such as inflows, outflows or merger events which affect the hydrostatic equilibrium within galaxies (e.g. Pérez-Díaz et al. 2024a; Sharda et al. 2024).

Since the pioneering works from Peimbert (1967); Peimbert & Costero (1969); Searle (1971); Searle & Sargent (1972), the chemical content of the gas-phase ISM is generally traced by the oxygen (O) abundance since it is the most abundant element in mass (~55%, Peimbert et al. 2007) and its presence helps cooling the nebula through emission lines detected in the ultraviolet (UV), optical (Opt) and infrared (IR) regimes, being the brightest ones those arising from collisional excitation. The oxygen abundance, expressed relative to hydrogen [$12+\log(\text{O}/\text{H})$], is af-

ected by flow dynamics which can alter one or both quantities. Hence, complementary information is required to constrain the chemical enrichment stage of the ISM. In a simplified picture of the complex nucleosynthesis of elements such as nitrogen (N) and carbon (C), they are produced by massive stars (primary), but an additional channel of production arises when oxygen is already present in the ISM from which intermediate mass stars were born, allowing them to produce N and C via CNO cycles (secondary, e.g. Henry et al. 2000). Complexity arises from other important aspects in chemical evolution models such as the time delay of ISM pollution from intermediate mass stars (e.g. Vincenzo et al. 2016), the role of fast-rotator stars (e.g. Grisoni et al. 2021) or variations in the star-formation histories (e.g. Mollá et al. 2006). Thus, analyzing $\log(\text{N}/\text{O})$ and/or $\log(\text{C}/\text{O})$ ratios we gain additional information to constrain the chemical enrichment history in galaxies.

The presence of these elements in the gas-phase ISM helps its cooling by emission lines which are used to estimate the chemical content. Recipes to estimate chemical abundances in the gas-phase ISM have been proposed, exploited and perfected over the last decades. All of them can be summarized in three main groups. The first one relies on using auroral emission lines,

such as [O III] λ 4363Å, [N II] λ 5755Å and/or [S III] λ 6312Å as well as other collisionally excited lines (CEIs) to constrain the physical properties of the gas-phase ionized ISM such as electron temperature (T_e) and density (n_e), which is called the direct method or T_e -method (e.g. Pérez-Montero & Amorín 2017). Some problems that arise from this method are i) the faint nature of such auroral emission lines, ii) the lack of emission lines from high-ionized species (e.g. [OIV], [SIV], [NeV]) in the optical range imposes an assumption on the ionization correction factors (ICFs) and, iii) fluctuations of the physical properties required such as temperature might induce systematic uncertainties in their determination (Méndez-Delgado et al. 2023), although some ratios such as $\log(N/O)$ are not affected by these fluctuations. The second technique relies on the use of photoionization models such as CLOUDY (Ferland et al. 2017), MAPPINGS (Sutherland & Dopita 2017) or SUMA (Contini & Aldrovandi 1983), in which both the physical and the chemical conditions in the gas-phase ISM as well as the source of ionization are given and then they are constrained either to directly match the observations with tailor-made models (e.g. Pérez-Montero et al. 2010) or by bayesian approaches such as HII-CHI-MISTRY (HCM, Pérez-Montero 2014), NEBULABAYES (Thomas et al. 2018) or HOMERUN (Marconi et al. 2024). Finally, a different technique but more spread due to its easy applicability is the use of strong emission line ratios or combinations that correlate with the chemical abundances, which are calibrated by using one of the other two previous techniques. A summary on these calibrators can be found in Tab. 1 from Maiolino & Mannucci (2019).

The above mentioned techniques have been used over decades (McClure & van den Bergh 1968; Lequeux et al. 1979; Vilchez et al. 1988; Thuan et al. 1995; Pérez-Montero & Díaz 2005; Andrews & Martini 2013; Fernández-Ontiveros et al. 2021), specially for analyzing the chemical composition of the gas-phase ISM in star-forming dominated galaxies (SFGs) over different cosmic times from either slit spectroscopy or integral field spectroscopy. However, to properly constrain galaxy chemical evolution studies cannot focus only on SFGs, but they also need to study galaxies hosting Active Galactic Nuclei (AGNs), which have an important role not only on galaxy evolution (e.g. Page et al. 2004; de Nicola et al. 2019) as AGN feedback affects gas cooling and consequently star formation (Morganti 2017; Capelo et al. 2023), but also in cosmological structures (e.g. Gitti et al. 2012; Eckert et al. 2021; Nobels et al. 2022). However, studies on the chemical content of the gas-phase ISM within galaxies hosting AGNs are rather scarce. The gas-phase ISM surrounding the Super Massive Black Hole (SMBH) in AGNs is divided in two different regions: the Broad Line Region (BLR) located close ($r \sim 0.01$ pc Mandal et al. 2021) to the SMBH and characterized by high densities ($n_e > 10^9$ cm $^{-3}$) and broad emission line components (> 1000 km/s) (Peterson 2006); and the Narrow Line Region located at greater distances ($r \gtrsim 1$ pc Peterson et al. 2013), lower densities ($n_e \sim 10^3$ cm $^{-3}$) and narrower emission line components (~ 500 km/s) (Peterson 2006). The BLR present several problems for the estimation of its abundance composition both observationally due to the high covering factors (Gaskell 2009) and theoretically due to the complex gas dynamics governing its motion (Gaskell 2009) or even the high variability in the broad emission lines that trace the BLR (Ilić et al. 2017). These problems disappear when considering the NLR due to the fact the physical properties are much similar to those of HII regions.

Nevertheless, determination of chemical abundances in the NLR present some caveats. It has been shown by Dors et al. (2015) that the use of the direct method to constrain chemi-

cal abundances yields unexpectedly low chemical abundances that are not found using other techniques. Moreover, the lack of detection in the optical of emission lines from highly-ionized species, which are expected due to the harder ionizing front from the AGN (Pérez-Díaz et al. 2022, 2024a), adds more uncertainty to its estimations. Hence, most of the techniques to study chemical abundances in the NLR of AGNs rely on either using photoionization models to directly estimate their abundances or to either provide calibrations to estimate them in larger samples (e.g. Pérez-Montero et al. 2019; Carvalho et al. 2020; Pérez-Díaz et al. 2021, 2022; Dors et al. 2023).

An additional bias in the studies of chemical abundances in AGNs is that they target mainly Seyferts 2, i.e., high ionized AGNs, whereas low-luminosity AGNs (LLAGNs), such as LINERs, are the most common type of AGN in the local Universe (Ho et al. 1997). The studies of chemical abundances in LLAGNs are even more unusual. One of the main reasons for such scarcity is the fact that there is no consensus in the literature about the source of ionization of LINERs. Among them we can find: i) sub-Eddington accretion (Kewley et al. 2006; Ho 2009) onto supermassive black holes (SMBHs) which can latter affect the flow of gas even truncating the disk through advected-dominated flows (ADAFs, Nemmen et al. 2014); ii) hot old stellar populations dominated by post-asymptotic giant branch (pAGB) stars (Binette et al. 1994; Stasińska et al. 2008); and, iii) fast radiative shocks (Dopita & Sutherland 1995; Allen et al. 2008).

Among the first works estimating oxygen abundances in a statistically significant sample of LLAGNs we found the study by Annibali et al. (2010), as they were targeting 67 early-type galaxies in the local Universe, most of them ($\sim 72\%$) hosting LINERs. However, they rely on calibrations that were obtained from photoionization models assuming AGNs (Storchi-Bergmann et al. 1998) as source of ionization or on empirical calibrations taken from the analysis of early-type galaxies which would mimic the conditions in their sample (Kobulnicky et al. 1999). Their resulting oxygen abundances were in the range $8.49 < 12+\log(O/H) < 9.01$, being the majority of them slightly supra-solar¹.

More recently, (Pérez-Díaz et al. 2021) made a systematic analysis of 16 Seyferts 2 and 40 LINERs from the Palomar Spectroscopic Survey (Ho et al. 1997), complemented by an additional sample of 25 LINERs from (Pović et al. 2016). To estimate oxygen abundances the authors employed HII-CHI-MISTRY (hereinafter HCM, Pérez-Montero 2014; Pérez-Montero et al. 2019), a bayesian-like code which relies on a large grid of photoionization models, assuming AGNs as source of ionization as they found that multiwavelength studies pointed towards AGN feature emissions in X-rays and radio wavelengths. They reported that some ($\sim 15\%$) LINERs were characterized by unexpectedly low oxygen abundances ($12+\log(O/H) < 8.3$). Later on, Oliveira et al. (2022) present an analysis of the nuclear region of 43 LINERs from the SDSS IV - MaNGA survey (Bundy et al. 2015; Blanton et al. 2017) from photoionization models assuming pAGB stars as source of ionization, concluding that their sample of LINERs is characterized by solar-like oxygen abundances $8.54 < 12+\log(O/H) < 8.84$. A similar result was found in a recent study by Oliveira et al. (2024a), reporting that weak-AGNs present oxygen abundances in the range $8.50 < 12+\log(O/H) < 8.90$. Only the study by (Krabbe et al. 2021), an-

¹ Hereinafter, we assume the solar abundances reported by Asplund et al. (2009), e.g., $12+\log(O/H)_\odot=8.69$, $12+\log(N/H)_\odot=7.83$ and $\log(N/O)_\odot=-0.86$

alyzing just one LINER galaxy (UGC 4805) using also MaNGA data and photoionization models, simultaneously explored the AGN and the pAGBs ionizing scenarios. While their finding of metallicity trends did not provide a concluding clue, they suggest that the pAGB scenario is the most favorable, considering the position of this nucleus on some specific diagnostic diagrams for the observed emission lines, as well as the observed high degree of ionization.

The realm of analysis of nitrogen abundances in LLAGNs is even more scarce. Apart from the pioneering work from Pérez-Díaz et al. (2021), only the recent work by Oliveira et al. (2024b) analyzes the $\log(\text{N/O})$ abundance ratio and its relation with the $12+\log(\text{O/H})$ abundance in order to constrain the chemical enrichment of these objects. Although both studies employed photoionization models, assuming different ionizing sources (AGNs and pAGBs respectively), the results were consistent, showing that LINERs tend to have slightly higher $\log(\text{N/O})$ than those reported in SFGs.

Exploiting the capabilities of integral field spectroscopic (IFS) data from SDSS IV - MaNGA survey (Bundy et al. 2015; Blanton et al. 2017), we present a series of papers analyzing the spatially resolved chemical enrichment of the gas-phase ISM in galaxies hosting LINER-like nuclear emission, considering for the first time different scenarios that might explain the observed emission in a statistically significant sample of galaxies. This first paper of the series is focus on the determination of nuclear chemical abundances in this sample, and is organised as follows. In section 2, the selection of the sample of galaxies hosting LINER-like emission is explained as well as other different criteria used in this study. In section 3 we discussed the methodology employed to estimate chemical abundances in our sample. In section 4 we present the main results of this study and its a discussion in section 5. In section 6 we summarize the main conclusions. In this paper, we have assumed the cosmological parameters given by $\Omega_m = 0.3$, $\Omega_\Lambda = 0.7$ and $H_0 = 67$ km/s/Mpc.

2. Sample selection

2.1. MaNGA data and emission line measurements

The Mapping Nearby Galaxies at Apache Point Observatory (MaNGA; Bundy et al. 2015) is part of the Sloan Digital Sky Survey IV (SDSS IV; Blanton et al. 2017). For this work, we used data release 17 (DR17, Abdurro'uf et al. 2022). We used individual spaxels whose size is significantly smaller than that of the point spread function (PSF) in the MaNGA datacubes. The spatial resolution of these cubes has a median full width at half maximum (FWHM) of 2.54 arcsec (Law et al. 2016).

We examined the MaNGA spectra as outlined in Zinchenko et al. (2016, 2021). Briefly, we used the STARLIGHT code (Cid Fernandes et al. 2005; Mateus et al. 2006; Asari et al. 2007) to fit the stellar background across all spaxels, adapting it for parallel datacube processing. Simple stellar population (SSP) spectra from Bruzual & Charlot (2003) evolutionary synthesis models were used for stellar fitting, and we subtracted this from the observed spectrum for a pure gas spectrum. Then, we fit emission lines using our ELF3D code. Each emission line was fit with a single-Gaussian profile. For each spectrum, we measured the fluxes of the $[\text{O II}]\lambda, \lambda 3726, 3729\text{\AA}$ (hereinafter $[\text{O II}]\lambda 3727\text{\AA}$), $[\text{Ne III}]\lambda 3868\text{\AA}$, H_β , $[\text{O III}]\lambda 4959\text{\AA}$, $[\text{O III}]\lambda 5007\text{\AA}$, $[\text{N II}]\lambda 6548\text{\AA}$, H_α , $[\text{N II}]\lambda 6584\text{\AA}$, and $[\text{S II}]\lambda, \lambda 6717, 6731\text{\AA}$ lines with a signal-to-noise ratio $S/N > 3$.

2.2. Sample classification

From the original sample of galaxies presented in the SDSS IV - MaNGA survey, we initially selected those galaxies that are classified as LINERs in at least one of the three diagnostic (BPT) diagrams (Baldwin et al. 1981; Veilleux & Osterbrock 1987) with the semiempirical constraints proposed by Kauffmann et al. (2003) and Kewley et al. (2006). For that purpose, we used emission lines H_β , $[\text{O III}]\lambda 5007\text{\AA}$, $[\text{O I}]\lambda 6300\text{\AA}$, $[\text{N II}]\lambda 6584\text{\AA}$, $[\text{S II}]\lambda 6717\text{\AA}$ and $[\text{S II}]\lambda 6731\text{\AA}$. Additionally, we complement the diagrams with information on the equivalent width (EW) for H_α , as proposed by Cid Fernandes et al. (2011) since the strength of these feature allows us to better distinct between galaxies whose activity is dominated by "strong" AGNs (sAGN, $W_{\text{H}_\alpha} > 6\text{\AA}$), "weak" AGNs (wAGN, $3\text{\AA} < W_{\text{H}_\alpha} < 6\text{\AA}$) and "retired galaxies" (RG, $0.5\text{\AA} < W_{\text{H}_\alpha} < 3\text{\AA}$). Below that limit, there is the region dominated by "passive galaxies" (PG, $W_{\text{H}_\alpha} < 3\text{\AA}$) which are mainly lineless galaxies (Cid Fernandes et al. 2011).

To perform the classification, we focused our attention on the central spaxel for each galaxy. The median distance for our sample of galaxies is 150.56 Mpc, within a range [35.24 Mpc, 560.09 Mpc], implying that the spaxel size is on average 1.460 kpc within a range of [0.342 kpc, 5.4 kpc] for the $2''$ fiber coverage in the sky (Bundy et al. 2015). This allows us to capture most of the emission in case an AGN is the source of ionization considering the average sizes of the Narrow Line Region ($\sim 1\text{-}5$ kpc Bennert et al. 2006a,b). This range is also valid to accommodate the case in which pAGB stars are ionizing the gas-phase ISM (e.g. Binette et al. 1994). While other authors integrate the flux in a circular aperture of 1 kpc radius (Oliveira et al. 2024b), we obtained that the average change in the emission line flux ratios is less than 5%, thus the classification and later results are not affected by selecting either the central spaxel or 1 kpc aperture.

We show in Figure 1 the diagnostic diagrams for the central spaxels in our sample of galaxies from MaNGA. If we only consider those galaxies classified by at least one of the diagrams as LINERs, we came up with a sample of 429 galaxies. Considering that problems of contamination from diffuse ionized gas (DIG) in $[\text{S II}]$ are higher than in $[\text{N II}]$ lines (Pérez-Montero et al. 2023), we imposed that galaxies are classified as LINERs simultaneously in all three diagrams, reducing the sample to 329 galaxies, with values of W_{H_α} in the range [1.74 \AA , 9.25 \AA]. Since we cannot rule out the possibility of contamination from different ionizing sources (e.g. the combination of star formation and AGN activity, Davies et al. 2016), we complemented our classification with information from the WHAN diagram (Cid Fernandes et al. 2011). As shown in Figure 2, the majority of our galaxies fall in the "wAGN" region, with some galaxies presenting slightly higher or lower values. Only one galaxy is classified as SFG due to the weak ratio between H_α and $[\text{N II}]\lambda 6584\text{\AA}$. As it can be seen in Table 1, the majority of the sample falls in the "wAGN" region (300, $\sim 70\%$). If we focus our attention only on those galaxies classified as "LINERs" based on the BPT diagram (329, $\sim 77\%$), we find out that the percentage of "wAGN"-like galaxies is even higher than in the overall sample ($\sim 73\%$).

Another constraint added to the sample selection is that the detected LINER-like emission mainly comes from the central spaxel. By restricting our sample under this criterion, we ensure: i) that there are enough HII regions to analyse spatially resolved properties across the whole galaxies such as metallicity gradients (second paper of these series); ii) that the origin of the LINER-like emission cannot be automatically excluded as AGN originated; and, iii) we can test for the same galaxy what is hap-

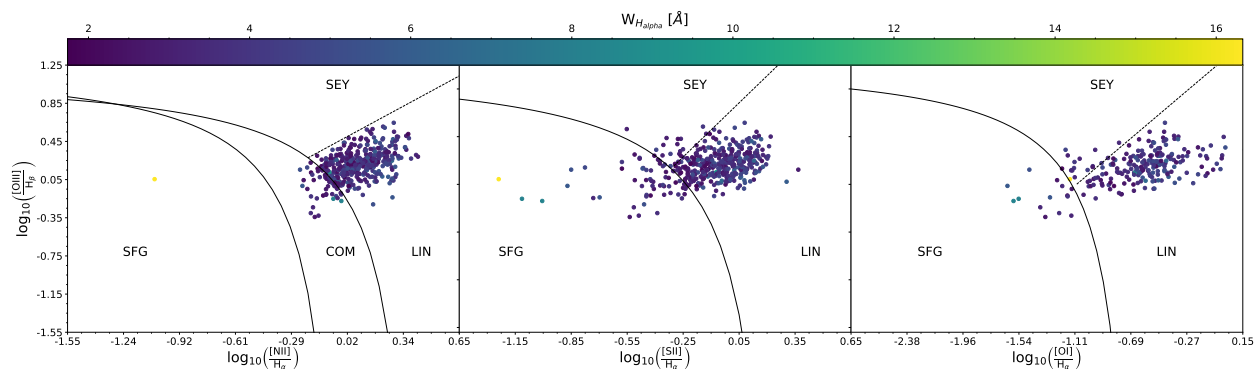


Fig. 1. Diagnostic diagrams of the central spaxels in our sample of galaxies. The colorbar shows the equivalent width for H_{α} ($W_{H_{\alpha}}$). Solid lines and dashed represent the region limits as defined by Kewley et al. (2006), with the exception of the separation between Seyferts 2 and LINERs in the $[NII]/H_{\alpha}$ diagram that was taken from Cid Fernandes et al. (2010). Each region is labeled as follows: "SFG" for star-forming galaxies; "SEY" for Seyferts; "LIN" for LINERs; and "COM" for composites.

Table 1. Classification of the central spaxels from the preliminary sample of 429 galaxies selected from MaNGA. The headline row shows the classifications based on the WHAN diagram (Cid Fernandes et al. 2010, 2011). The first column shows the classification based on the BPT diagrams (Kauffmann et al. 2003; Kewley et al. 2006). In parenthesis, the relative percentage per each group is provided.

Classification	SFG	sAGN	wAGN	RG	PG	Total
LINERs	0 (0.00)	7 (2.13)	239 (72.64)	83 (25.23)	0 (0.00)	329 (76.87)
Composites	0 (0.00)	2 (4.17)	26 (54.17)	20 (41.67)	0 (0.00)	48 (11.21)
Ambiguous	1 (1.96)	0 (0.00)	35 (68.63)	15 (29.41)	0 (0.00)	51 (11.92)
Total	1 (0.23)	9 (2.10)	300 (70.09)	118 (27.57)	0 (0.00)	428 (100.00)

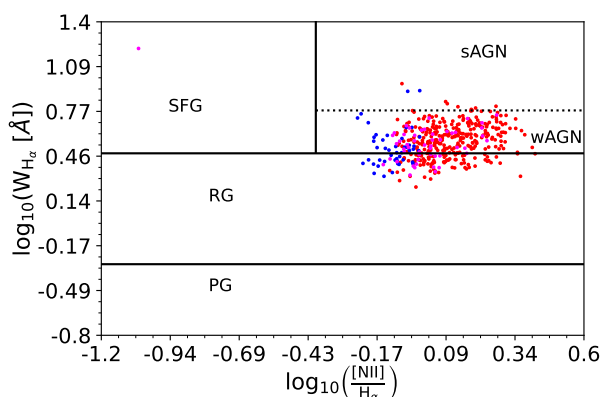


Fig. 2. The WHAN diagram showing the region demarcations as provided by Cid Fernandes et al. (2010, 2011). The color code represents the classification as given by the BPT diagrams (see Figure 1): red dots represent galaxies classified as LINERs, blue dots represent galaxies falling in the composite region and magenta dots are galaxies with no clear classification. Each region is labeled as follows: "SFG" for star-forming galaxies; "sAGN" for strong AGNs; "wAGN" for weak AGNs; "RG" for retired galaxies; and "PG" for passive galaxies.

pening in their SF-dominated regions as opposed to the nuclear region. By adding this constraint, we ended up with a sample of 105 galaxies, all of them showing LINER-like emission according to all BPT diagrams for the central spaxels. Among them, 57 are classified as "wAGN" and 48 as "retired galaxies" according to the WHAN diagram (Cid Fernandes et al. 2010, 2011).

3. Chemical abundance determination

In this section we present a detailed explanation on the methodology used to estimate chemical abundances as well as other physical parameters from the nebular emission retrieved from

the MaNGa data. As we are accounting for possible different natures of the ionizing source in the nuclear regions of our sample of galaxies, we simultaneously analyzed all these scenarios by means of photoionization models.

3.1. HII-CHI-Mistry

To estimate chemical abundances we rely on the bayesian-like python code HII-CHI-MISTRY² (or HCM), developed by Pérez-Montero (2014) originally for HII regions, but later on extended to AGN sources (Pérez-Montero et al. 2019; Pérez-Díaz et al. 2021) and extreme emission line galaxies (Pérez-Montero et al. 2021) for the optical version. We made use of the optical version 5.5 of the code. HCM uses a grid of photoionization models with three free parameters the chemical properties of the gas-phase ISM $12+\log(O/H)$ and $\log(N/O)$ as well as the ionization parameter $\log(U)$ by comparing emission line ratios sensitive to those parameters. Other important properties for the computation of photoionization models such as geometry, density, dust-to-gas ratio, stopping criteria are explored for each grid of models. In a first iteration, the code estimates $\log(N/O)$ and uses that estimation to constrain the grid of models. This first estimation is always done as we have all necessary emission lines for such determination (e.g. $[O\ II]\lambda 3727\text{\AA}$, $[N\ II]\lambda 6584\text{\AA}$). In a second iteration, the code performs an estimation of $12+\log(O/H)$ and $\log(U)$. Since all those parameters are free in the grid of models, the estimation of all quantities is done independently from each other, without the assumption of a relation between them.

We used as input for HCM the emission line ratios $[O\ II]\lambda 3727\text{\AA}$, $[Ne\ III]\lambda 3868\text{\AA}$, $[O\ III]\lambda 5007\text{\AA}$, $[N\ II]\lambda 6584\text{\AA}$ and $[S\ II]\lambda 6717\text{\AA}+[S\ II]\lambda 6731\text{\AA}$, referred to H_{β} emission. All emission line ratios were corrected from reddening assuming Case

² The code is publicly available at <http://home.iaa.csic.es/~epm/HII-CHI-mistry.html>.

B photoionization and an expected ratio between H_α and H_β of 3.1 for standard conditions in the NLR, i.e., electron density $n_e \sim 500 \text{ cm}^{-3}$ and electron temperature $T_e \sim 10^4 \text{ K}$ (Osterbrock & Ferland 2006) and the extinction curve from Howarth (1983) for $R_V = 3.1$.

3.2. Grids of photoionization models

Whereas HCM allows us to perform the same methodology with independence of the source of ionization, as the user must select the grid of photoionization models used in the estimation, the differences will emerge from the assumed spectral energy distribution (SED). All models were computed using CLOUDY³ v17 (Ferland et al. 2017)

In the case of HII regions, we chose as ionization source a cluster of star formation with an age of 1 Myr, using POPSTAR (Mollá et al. 2009) synthseis code for an initial mass function (IMF) that follows the trend reported by Chabrier (2003). The gas density is assumed to be 100 cm^{-3} . By allowing the variation of the ionization parameter and metallicity, Pérez-Montero (2014) demonstrated that these models are able to reproduce the emission line ratios observed in HII regions.

In the case of the nuclear emission, we built different grids of photoionization models that account for all scenarios proposed to reproduce the LINER-like emission:

- AGN SEDs composed by two components: the first one represents the Big Blue Bump peaking at 1 Ryd, and the other a power law with spectral index $\alpha_X = -1$ representing the non-thermal X-rays radiation. To test different regimes in the hardness of the ionization, we selected several values for the slope in the power law tracing the continuum between 2.5 keV and 2500 \AA (α_{OX}) given by $\alpha_{OX} = [-0.8, -1.0, -1.2, -1.4, -1.6, -1.8, -2.0]$. Although it has been reported that slopes below $\alpha_{OX} = -1.4$ do not reproduce well the observed emission line ratios (Carvalho et al. 2020; Oliveira et al. 2024a), we explore all these scenarios to search for significant differences due to the choice of this parameter.
- pAGB SEDs obtained from the grid of non local thermodynamic equilibrium (NLTE) model atmospheres⁴ provided by (Rauch 2003) for three different effective temperatures: $5 \cdot 10^4 \text{ K}$, $1 \cdot 10^5 \text{ K}$ and $1.5 \cdot 10^5 \text{ K}$. These SEDs were computed assuming $\log g = 6$ and normalized fractions of 0.33 for helium, 0.50 for carbon, 0.02 for nitrogen and 0.15 for oxygen.
- An advected-dominated accretion flow (ADAF) model for the AGN, which represents the truncation of the accretion disk due to inefficiency in the accretion process. Particularly, we made use of the code RIAF-SED⁵ (Yuan et al. 2005, 2007; Nemmen et al. 2014). Considering the large number of free parameters for the computation, we used the average SED that characterized ADAF emission in LLAGN (see Nemmen et al. 2014, for more details).

For each considered SED, we modeled the ISM allowing the oxygen abundance to vary in the range $6.9 < 12 + \log(\text{O}/\text{H}) < 9.1$ in steps of 0.1 dex, the nitrogen-to-oxygen ratio varies in the range $-2.0 < \log(\text{N}/\text{O}) < 0.0$ in steps of 0.125 dex and the ionization parameter in the range $-4.0 < \log(U) < -0.5$ in steps

of 0.25 dex. This last parameter is preliminary constrained in the range $-4.0 < \log(U) < -2.5$, according to previous findings (e.g. Pérez-Díaz et al. 2021; Oliveira et al. 2022, 2024b), as it is needed to break the degeneracy reported in some emission line ratios Pérez-Montero et al. (2019); Pérez-Díaz et al. (2021). For all models, a density of 500 cm^{-3} is assumed. In total, we computed 4928 models per ionizing source, which yields a total of 54208 models. We also explored the effects of the stopping criteria by considering two different scenarios: when the ratio ionized hydrogen atoms is 0.98 and 0.02. As already reported by other studies (e.g. Pérez-Díaz et al. 2021, 2022), these two scenarios do not introduce significant differences (they are lower (~ 0.05 dex) than the steps in the grid of models) in the chemical abundance estimations.

4. Results

4.1. Oxygen and nitrogen abundances

In Tables 2 and 3 we provide the overall statistics for the derived oxygen abundance and nitrogen-to-oxygen abundance ratio respectively, in our selected sample of LINERs. We give the results for each considered ionizing source in the models used to calculate the abundances for the whole sample, and also segregating them according to their classification as wAGN or as retired galaxies (RG).

Focusing our attention on $12 + \log(\text{O}/\text{H})$, we can see that there is no difference between the median values derived for wAGN and RGs (~ 0.05 dex, lower than the grid step and compatible within the errors), being always close to the solar value ($12 + \log(\text{O}/\text{H}) \sim 8.69$, Asplund et al. 2009). Only in the case of the ADAF models, we obtained subsolar median values but still no significant difference was found between the two families. Particularly interesting is the case of assuming pAGB models ($T_{\text{eff}} = 1 \cdot 10^5 \text{ K}$ and $T_{\text{eff}} = 1.5 \cdot 10^5 \text{ K}$), as the difference between the resulting median values in each family increases (~ 0.1 dex), although they are still compatible within the errors. Overall, we see that the lower values of oxygen abundance are found in those galaxies classified as RG, with values ~ 0.3 dex below the solar abundance. If pAGB models are considered, then both distributions reach subsolar values, below ~ 0.4 dex for wAGN and ~ 0.6 dex for RGs. This differentiation between AGN (and ADAF) models and pAGB models is highlighted in Fig. 3.

Examining the $\log(\text{N}/\text{O})$ ratio, we find a completely different picture to that depicted for oxygen. For a given particular model, we can observe that $\log(\text{N}/\text{O})$ behaves on a statistically similar way for both groups of galaxies (differences below 0.06 dex). For a given group, there is little difference between the N/O ratios obtained assuming distinct AGN models. When considering either pAGB or ADAF models, there is an increase in the median value with respect to AGN models (~ 0.15 dex). Nevertheless, they are still compatible considering the standard deviations of the distributions. Overall, we found that median values cluster around the solar abundance ratio ($\log(\text{N}/\text{O}) \sim -0.86$, Asplund et al. 2009), but there is a wider range of values (~ 0.9 dex) than that observed for $12 + \log(\text{O}/\text{H})$ (~ 0.4 dex). In Fig. 4 we show the distributions of the $\log(\text{N}/\text{O})$ estimations for each group and for the whole sample, showing that there is little difference among them and for each photoionization grid of models.

As shown in Fig. 3 (see also Table 2), oxygen abundances estimated from pAGB models with temperatures as low as $T_{\text{eff}} = 5 \cdot 10^4 \text{ K}$ spread over a very narrow range of values [8.4, 8.6], which is even shorter than that observed from the ADAF models. A closer look to the photoionization models reveal that no O^{3+} is

³ The code is publicly available at <https://gitlab.nublado.org/cloudy/cloudy>.

⁴ They can be downloaded from http://astro.uni-tuebingen.de/~rauch/TMAF/flux_H-Ca.html.

⁵ The code is publicly available at <https://github.com/rsnemmen/riaf-sed>.

Table 2. Properties of the resulting distribution of the derived oxygen abundances.

Model (1)	Class. (2)	$12+\log(\text{O}/\text{H})_{med}$ (3)	$12+\log(\text{O}/\text{H})_{sd}$ (4)	$12+\log(\text{O}/\text{H})_{min}$ (5)	$12+\log(\text{O}/\text{H})_{max}$ (6)
AGN $\alpha_{OX} = -0.8$	wAGN	8.72	0.05	8.59	8.84
	RG	8.71	0.08	8.36	8.82
	All	8.72	0.06	8.36	8.84
AGN $\alpha_{OX} = -1.0$	wAGN	8.66	0.04	8.54	8.77
	RG	8.64	0.07	8.36	8.76
	All	8.65	0.06	8.36	8.77
AGN $\alpha_{OX} = -1.2$	wAGN	8.57	0.05	8.47	8.68
	RG	8.59	0.04	8.46	8.64
	All	8.58	0.04	8.46	8.68
AGN $\alpha_{OX} = -1.4$	wAGN	8.70	0.05	8.57	8.79
	RG	8.66	0.07	8.37	8.75
	All	8.68	0.07	8.37	8.79
AGN $\alpha_{OX} = -1.6$	wAGN	8.70	0.05	8.59	8.78
	RG	8.64	0.08	8.32	8.78
	All	8.69	0.07	8.32	8.78
AGN $\alpha_{OX} = -1.8$	wAGN	8.70	0.05	8.55	8.78
	RG	8.64	0.08	8.31	8.76
	All	8.68	0.07	8.31	8.78
AGN $\alpha_{OX} = -2.0$	wAGN	8.70	0.05	8.54	8.79
	RG	8.64	0.08	8.30	8.76
	All	8.69	0.08	8.30	8.79
pAGB $T_{eff} = 5 \cdot 10^4$ K	wAGN	8.47	0.02	8.41	8.55
	RG	8.47	0.02	8.44	8.53
	All	8.47	0.02	8.41	8.55
pAGB $T_{eff} = 1 \cdot 10^5$ K	wAGN	8.64	0.11	8.28	8.74
	RG	8.50	0.14	8.07	8.74
	All	8.57	0.13	8.07	8.74
pAGB $T_{eff} = 1.5 \cdot 10^5$ K	wAGN	8.56	0.16	8.25	8.82
	RG	8.41	0.16	8.08	8.72
	All	8.50	0.17	8.08	8.82
ADAF	wAGN	8.51	0.04	8.43	8.60
	RG	8.50	0.04	8.42	8.62
	All	8.51	0.04	8.42	8.62

Notes. For each photoionization model (1) and each group of LINERs (2) the median value (3), standard deviation (4), minimum (5) and maximum values (6) are provided.

predicted by these models in the nebulae, due to their relatively softer ionizing incident field of radiation. Hence, in order to properly provide a simultaneous estimation of the oxygen abundance (mainly traced through the sum of O^{++} and O^+ emission lines) and the ionization parameter (mainly traced through the ratio of O^{++} and O^+ emission lines), these models with a lower effective temperatures constrain the obtained oxygen abundance in a more restricted range, contrary to other models with higher T_* that allow a larger variation of the same involved lines, as these same models predict a higher abundance of other higher ionized species such as O^{3+} .

4.2. N/O vs O/H relation

The $\log(\text{N}/\text{O})$ vs $12+\log(\text{O}/\text{H})$ relation allows us to check whether the ISM is following a standard chemical enrichment history, characterized by constant $\log(\text{N}/\text{O})$ values at low metallicities ($12+\log(\text{O}/\text{H}) < 8.6$, Belfiore et al. e.g. 2015) due to the primary production of N and a positive increasing correlation at higher metallicities due to the contribution of the secondary production in intermediate massive stars (e.g. Vila-Costas &

Edmunds 1993; Coziol et al. 1999; Andrews & Martini 2013; Belfiore et al. 2015; Vincenzo et al. 2016).

We show in Fig. 5 the observed behavior in the N/O vs O/H diagram for our estimations of nuclear abundances in our sample of LINERs. Generally, we observe that no distinction is found between galaxies classified as wAGN or RG. Focusing on AGN models, we find that while our galaxies fall in the region delimited by the scatter in the literature, there seems to be an anticorrelation, with the exception of the estimations provided by AGN models with $\alpha_{OX} = -1.2$. The Pearson's coefficient correlation for those models are in the $[-0.57, -0.11]$ while the p-values are lower than 0.05 in most of the cases (with the exception of AGN models with $\alpha_{OX} = -0.8$), indicating that there is indeed such an anticorrelation. When pAGB models are considered (excluding those with low effective temperature), these coefficients are even higher, ~ -0.62 with pAGB models of $T_{eff} = 1 \cdot 10^5$ K and ~ -0.70 with pAGB models of $T_{eff} = 1.5 \cdot 10^5$ K, while p-values are even lower than 0.0005.

ADAF models and AGN models with $\alpha_{OX} = -0.8$ and $\alpha_{OX} = -1.2$ seem to follow the reported relation for SFGs, but their Pearson's coefficient correlation reveal that we cannot exclude the possibility that there is no correlation at all.

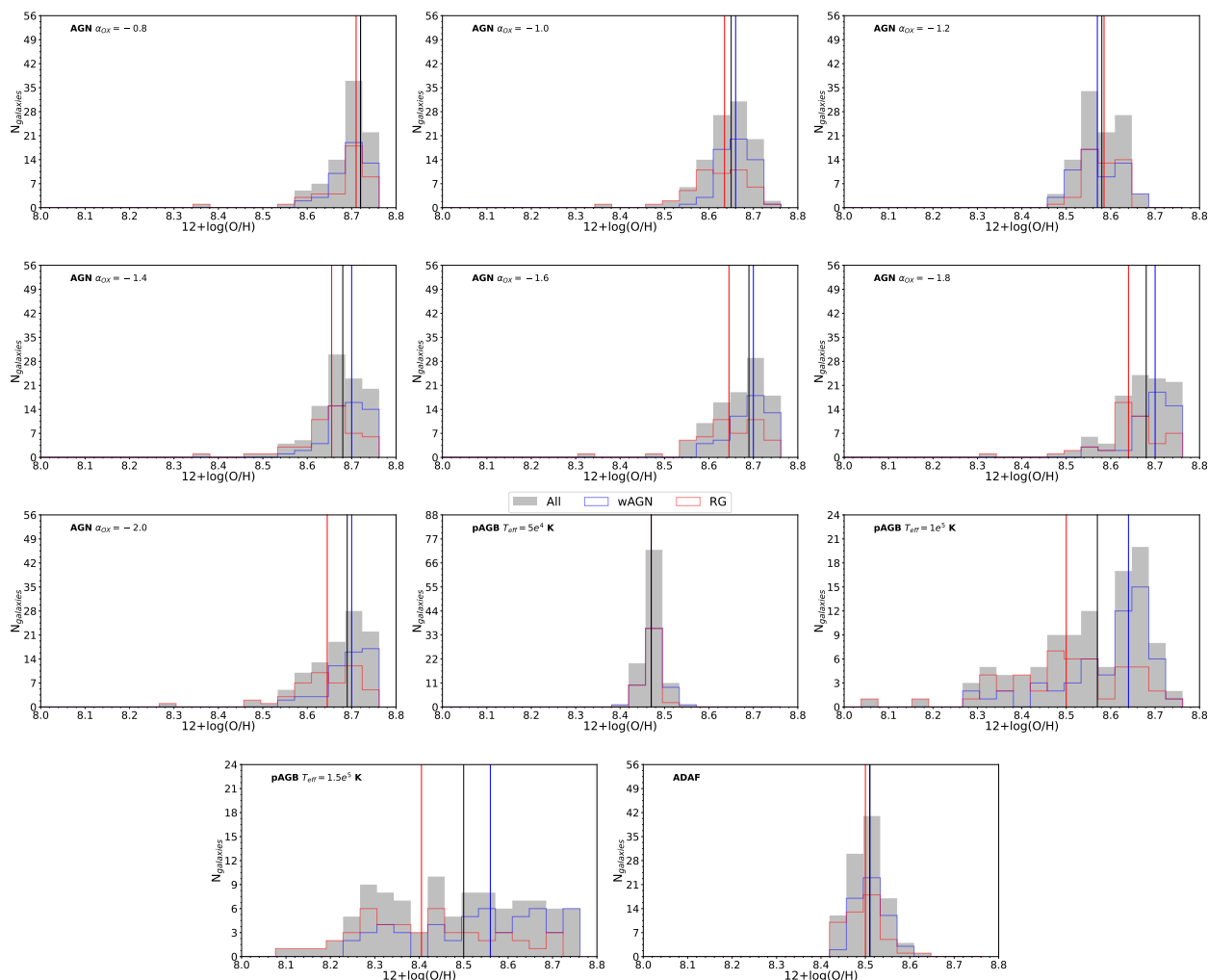


Fig. 3. Histograms for $12+\log(\text{O}/\text{H})$ nuclear abundance ratios for LINERs for each photoionization grid of models considered. Step-filled grey histogram corresponds to all LINERs in our sample. Step blue and red histograms correspond to wAGNs and RGs respectively. Vertical solid lines represent the median values for each distribution.

4.3. Mass-metallicity relation

Galaxy mass assembly is tied to the enrichment of the gas-phase ISM, as star formation leads to the production of metals which a fraction them can be later on ejected onto the surrounding ISM in their late stages of life. The well known mass-metallicity relation (MZR; Lequeux et al. 1979; Tremonti et al. 2004; Andrews & Martini 2013; Pérez-Montero et al. 2016) is a natural result that arises from this galaxy evolution scheme. While the use of oxygen abundance as tracer of the metallicity might lead to wrong conclusions, as it is the case when masses of inflow/outflowing gas are altering the ratio between oxygen and hydrogen (Köppen & Hensler 2005; Amorín et al. 2010; Pérez-Díaz et al. 2024a), the same analysis can be made using the nitrogen-to-oxygen abundance ratio as tracer of such metallicity (MNOR; Pérez-Montero & Contini 2009; Pérez-Montero et al. 2016), with the advantage that the same hydrodynamical processes that alter the MZR do not affect the MNOR.

In order to study these fundamental relations in our sample of galaxies, we retrieved the stellar mass data from the NASA-Sloan Atlas (NSA) catalogue⁶. These values were estimated from K-correction fit to the elliptical Petrosian fluxes assuming

⁶ <https://www.sdss4.org/dr17/manga/manga-target-selection/nsa/>.

the initial mass function (IMF) from Chabrier (2003) and the stellar population models from Bruzual & Charlot (2003).

As a general caveat, we used the abundance estimation from the nuclear region, whereas the reported relations are found when analyzing the chemical abundance estimation for the whole galaxy, which is more representative of the metallicity at effective radius (e.g. Sánchez-Menguiano et al. 2024) rather than the nuclear region. Nevertheless, this study gives insight on whether our derived chemical abundances and the relations between them in the nuclear region can be driven by galaxy physical parameters which are known to play a major role on their evolution.

We show in Fig. 6 the MZR in our sample of LINERs. First of all, we notice that some galaxies lie on the reported relation (Curti et al. 2020) for SFGs. This is specially true for AGN models, as we see that they cluster around the relation, although they show systematically lower metallicities (~ -0.15 dex). Analyzing the different subtypes of galaxies, we observe that although their host galaxies are characterized by stellar masses in the same range [$10^{9.8} M_{\odot}$, $10^{11} M_{\odot}$], the median value for RGs is lower ($10^{10.33} M_{\odot}$) than for wAGNs ($10^{10.63} M_{\odot}$). When considering pAGB with $T_{\text{eff}} = 5 \cdot 10^4$ K, the retrieved relation seems to lie quite below the reported relation and with little variation on metallicity, which highlights again the problem of assuming

Table 3. Same as Table 2 but for the nitrogen-to-oxygen abundance ratios $\log(\text{N/O})$.

Model (1)	Class. (2)	$\log(\text{N/O})_{med}$ (3)	$\log(\text{N/O})_{sd}$ (4)	$\log(\text{N/O})_{min}$ (5)	$\log(\text{N/O})_{max}$ (6)
AGN $\alpha_{OX} = -0.8$	wAGN	-0.88	0.16	-1.20	-0.39
	RG	-0.79	0.14	-1.15	-0.47
	All	-0.84	0.15	-1.20	-0.39
AGN $\alpha_{OX} = -1.0$	wAGN	-0.81	0.15	-1.14	-0.42
	RG	-0.74	0.14	-1.12	-0.43
	All	-0.78	0.15	-1.14	-0.42
AGN $\alpha_{OX} = -1.2$	wAGN	-0.82	0.15	-1.17	-0.39
	RG	-0.73	0.14	-1.08	-0.44
	All	-0.79	0.15	-1.17	-0.39
AGN $\alpha_{OX} = -1.4$	wAGN	-0.83	0.15	-1.19	-0.40
	RG	-0.75	0.14	-1.11	-0.50
	All	-0.79	0.15	-1.19	-0.40
AGN $\alpha_{OX} = -1.6$	wAGN	-0.84	0.16	-1.22	-0.38
	RG	-0.74	0.13	-1.11	-0.48
	All	-0.79	0.15	-1.22	-0.38
AGN $\alpha_{OX} = -1.8$	wAGN	-0.83	0.15	-1.18	-0.38
	RG	-0.75	0.14	-1.12	-0.47
	All	-0.81	0.15	-1.18	-0.38
AGN $\alpha_{OX} = -2.0$	wAGN	-0.83	0.15	-1.19	-0.38
	RG	-0.75	0.14	-1.11	-0.47
	All	-0.80	0.15	-1.19	-0.38
pAGB $T_{eff} = 5 \cdot 10^4$ K	wAGN	-0.63	0.13	-0.93	-0.33
	RG	-0.56	0.12	-0.88	-0.33
	All	-0.58	0.13	-0.93	-0.33
pAGB $T_{eff} = 1 \cdot 10^5$ K	wAGN	-0.71	0.15	-1.05	-0.24
	RG	-0.62	0.13	-1.00	-0.34
	All	-0.67	0.15	-1.05	-0.24
pAGB $T_{eff} = 1.5 \cdot 10^5$ K	wAGN	-0.71	0.15	-1.06	-0.27
	RG	-0.64	0.14	-1.00	-0.37
	All	-0.70	0.15	-1.06	-0.27
ADAF	wAGN	-0.74	0.15	-1.07	-0.27
	RG	-0.65	0.13	-0.99	-0.36
	All	-0.70	0.15	-1.07	-0.27

low effective temperatures for the ionizing source. When other pAGB models are considered, we retrieved no relation at all between mass and metallicity.

The picture that arises from the MNOR (Fig. 7) complements our result from the $\log(\text{N/O})$ vs $12+\log(\text{O/H})$ relation. First of all, there is very little difference in the obtained relations as a function of the assumed models. Secondly, most of our sample lies above the reported relation (Andrews & Martini 2013). This is consistent with the anomalous relation observed in Fig. 5: while oxygen abundances might be consistent (or slightly lower) with their corresponding mass, there is an increase in nitrogen-to-oxygen abundance ratio respect to the expected one, which points to a more complex scenario for the N evolution.

4.4. Comparison with the extrapolation from galaxy gradients

Although this procedure and all its associated results will be discussed in the forthcoming paper of this series, we briefly explain here the procedure for estimating metallicity gradients in the same galaxies hosting the nuclear regions classified as LINERs. First of all, we selected in each galaxy those spaxels classified as HII regions according to the three diagnostic diagrams (Baldwin et al. 1981; Kewley et al. 2006). Secondly, we used HCM to consistently derive metallicities for each HII region us-

ing POPSTAR as ionizing source in the models (see Sec. 3 for more details. Finally, for both $12+\log(\text{O/H})$ and $\log(\text{N/O})$ we used a piecewise methodology (Tapia, Tissera private communication) to estimate the metallicity gradient only accounting for HII regions, and allowing the profile to present breaks. Gradients were calculated normalizing distances to the R_{50} radius, azimuthally averaged SDSS-style Petrosian containing 50% light radius from the r-band.

From Fig. 8 we conclude that, in the case of $12+\log(\text{O/H})$, the extrapolations from the gradients within galaxies and the estimations from the nuclear emission do not match as the distribution of the differences is wide (over 0.6 dex) even though the median difference is close to 0. We also obtained the highest offset and dispersion when chemical abundances from the nuclear regions were estimated using pAGB models. This result holds true for both groups of galaxies considered in this analysis (wAGNs and RGs). A completely different idea emerges from Fig. 9, obtaining that the extrapolations from the gradients and the nuclear estimations match for the $\log(\text{N/O})$ abundance ratio, leading to narrower distributions of the differences (~ 0.4 dex) and median differences much closer to 0.

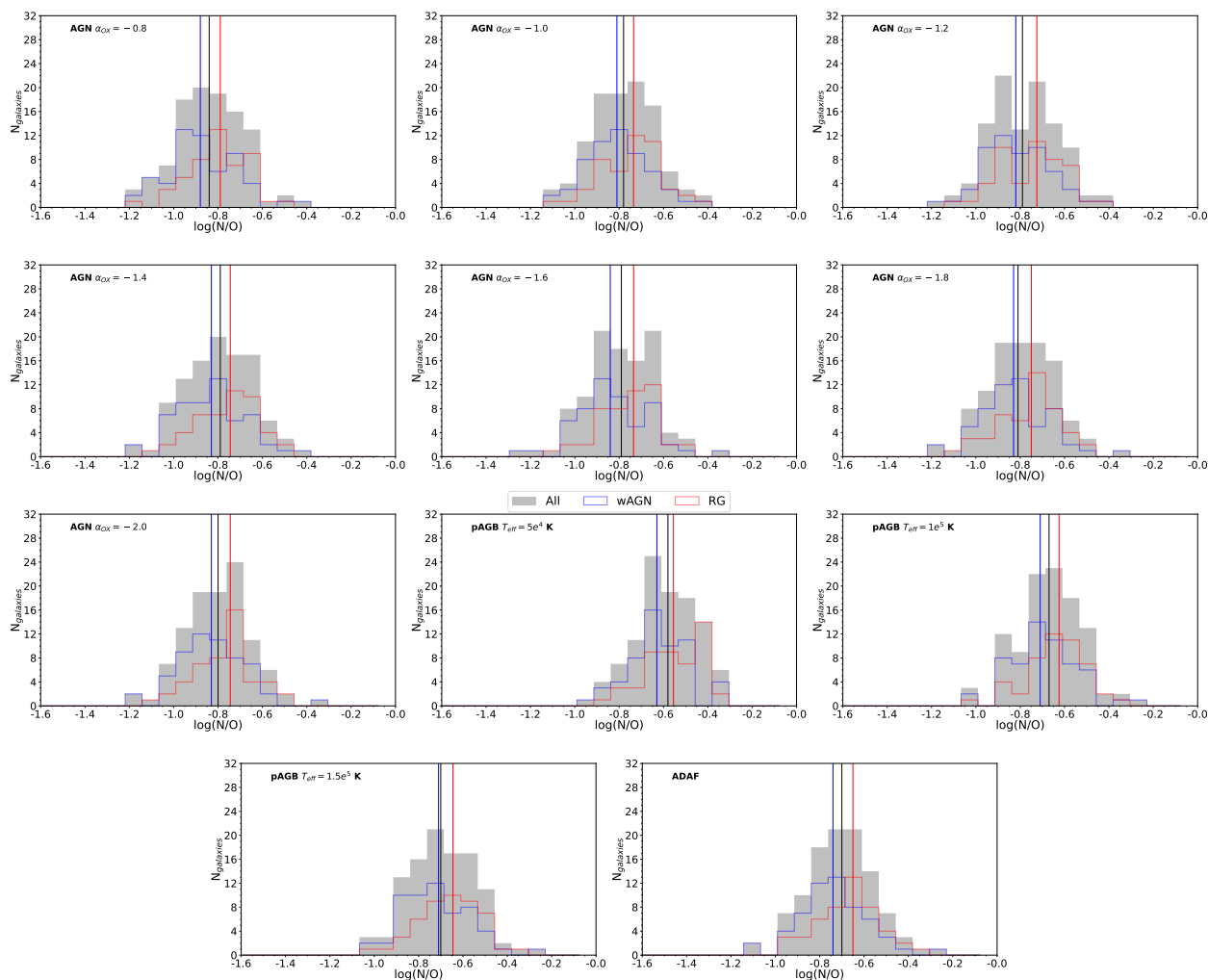


Fig. 4. Same as Fig. 3 but for $\log(\text{N}/\text{O})$ nuclear abundance ratios.

5. Discussion

In the following section we will omit the analysis of pAGB models with $T_{\text{eff}} = 5 \cdot 10^4$ K as it has been probed in Sec. 4 in agreement with previous works (e.g. Krabbe et al. 2021; Oliveira et al. 2022) that they are inefficient in reproducing the observed emission line ratios. Hence, through all this discussion when talking about pAGB models we will only refer to those characterized by $T_{\text{eff}} = 1 \cdot 10^5$ K and $T_{\text{eff}} = 1.5 \cdot 10^5$ K.

5.1. Comparison of the abundance estimations with the literature

Although the number of studies analyzing chemical abundances in LINERs is scarce (specially compared to SFG or Seyfert 2 studies), it is possible to compare our results with the few available so far in the literature.

Annibali et al. (2010) obtained that for their sample of early-type galaxies, when the Kobulnicky et al. (1999) (accounting for pAGN ionization) is used to estimate $12+\log(\text{O}/\text{H})$, the abundances reported in the nuclear region lie in the range [8.20, 9.01], which is in agreement to the results obtained for our sample of LINERs for all models. On the contrary, if the used calibration is that from Storch-Bergmann et al. (1998) (accounting for AGN activity), the range is constrained to [8.54, 8.94], as the validity range for such calibration is above $12+\log(\text{O}/\text{H}) > 8.4$. This

range also agrees to our findings when using AGN models as ionizing source, although we are able to retrieve lower values than are not traced by this calibration.

Oliveira et al. (2022) analyzed a sample of 43 LINERs from MaNGA classified as RGs in the WHAN diagram (Cid Fernandes et al. 2010, 2011). Assuming pAGB ionization, and by means of photoionization models, they used calibrations based on $\text{N}2$ ($\equiv [\text{N II}]\lambda 6584\text{\AA}/\text{H}\alpha$) and $\text{O}3\text{N}2$ ($\equiv [\text{O III}]\lambda 5007\text{\AA}/[\text{N II}]\lambda 6584\text{\AA}$) line ratios and obtaining oxygen abundances in the range [8.4, 8.84]. Contrary to our results, they did not obtain any LINER with $12+\log(\text{O}/\text{H}) < 8.4$ as we did, particularly in the case of RGs we obtained that 10 RGs (21%) show metallicities below that limit. When looking at their nitrogen-to-oxygen abundance ratio, we found that these group of low metal LINERs are also characterized by supra-solar $\log(\text{N}/\text{O})$ ratios [-0.67, -0.34]. Since the photoionization models built by Oliveira et al. (2022) assumed a relation between $\log(\text{N}/\text{O})$ and $12+\log(\text{O}/\text{H})$, their higher abundances might be interpreted as a consequence of using nitrogen emission lines as tracers of the oxygen abundance without an independent estimation of the $\log(\text{N}/\text{O})$ ratio, explaining this discrepancy.

A more recent study, provided by Oliveira et al. (2024b), shed more light on oxygen abundances in LINERs. Contrary to the previous work by Oliveira et al. (2022), they used tailor-made photoionization models to simultaneously constrain N and O abundances, without assuming any relation between them,

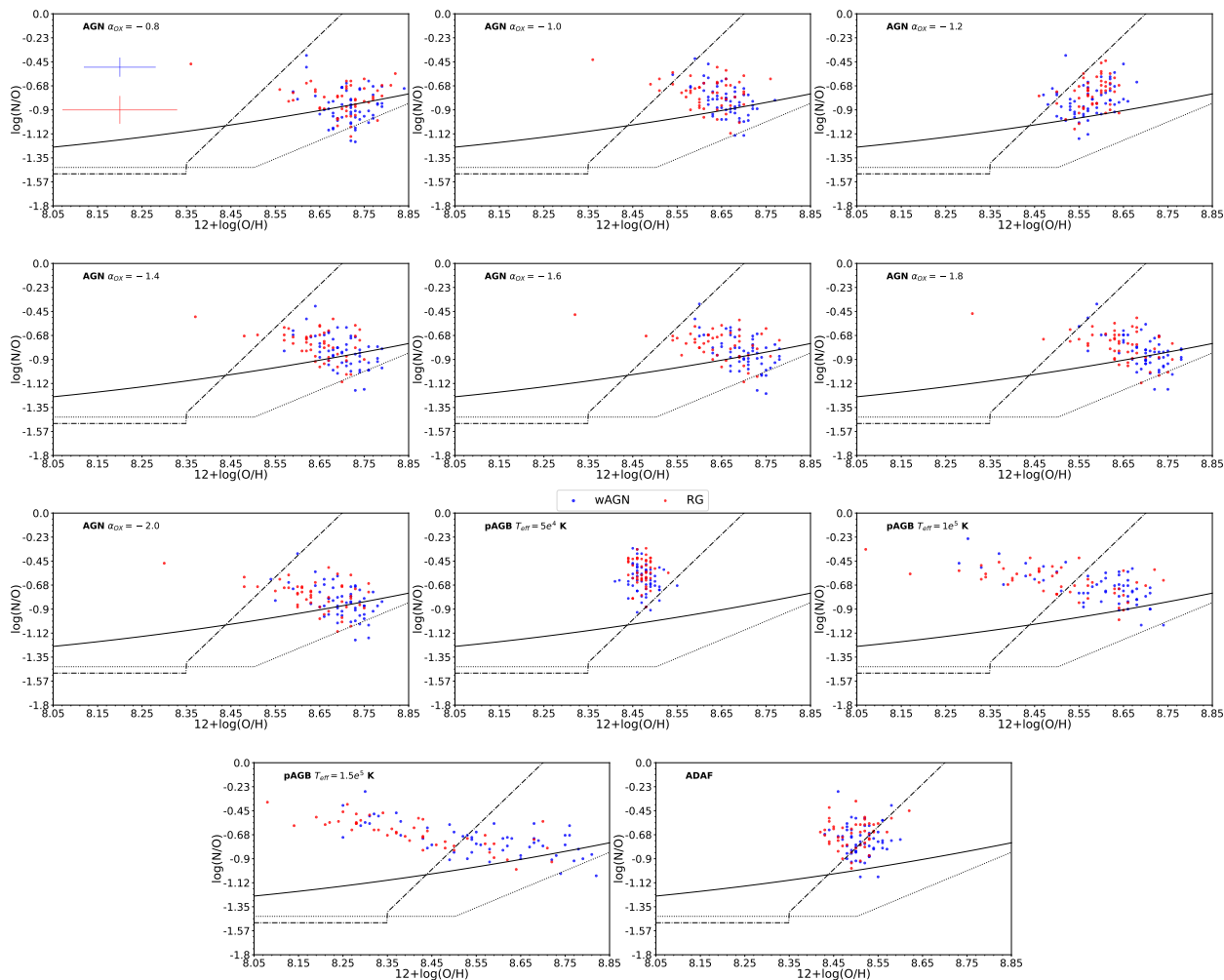


Fig. 5. Relation between the nuclear estimations of $\log(\text{N/O})$ and $12+\log(\text{O/H})$ nuclear estimations in our sample of LINERs for each grid of photoionization models. First plot shows the typical errors for the data. Solid back line represents the fit provided by Coziol et al. (1999), dotted line shows the fit by Andrews & Martini (2013) and dash-dotted line shows the fit by (Belfiore et al. 2015).

similar to our work. Their results from 40 out of the 43 previous RG LINERs on their oxygen content are on the range $8.0 \leq 12+\log(\text{O/H}) \leq 9.0$ which are similar to our findings, specially when pAGB models are considered for RGs ($8.07 \leq 12+\log(\text{O/H}) \leq 8.82$). However, there is a slight discrepancy between their mean value $12+\log(\text{O/H}) = 8.74$ and ours for RGs 8.57 (8.50) for pAGB models with $T_{\text{eff}} = 1 \cdot 10^5 \text{ K}$ ($T_{\text{eff}} = 1.5 \cdot 10^5 \text{ K}$). Even though they are still compatible within the errors, these discrepancy might be interpreted as a consequence of the fact that Oliveira et al. (2024b) considered dust-free photoionization models, whereas our grid of models accounts for a standard dust-to-gas ratio. Regarding nitrogen-to-oxygen abundance ratios, Oliveira et al. (2024b) reported a mean value of $\log(\text{N/O}) = -0.69 \pm 0.16$ with a range $[-1.05, -0.42]$, which are both in excellent agreement to ones we reported, although we detect few (3) LINERs with higher ratios.

Lastly, we also compared our results to those provided by Pérez-Díaz et al. (2021) analyzing 40 LINERs from the Palomar Spectroscopic Survey (Ho et al. 1993, 1997), using the same methodology as in this work but only considering AGN models with $\alpha_{\text{OX}} = -0.8$. They estimated a median $12+\log(\text{O/H}) = 8.63 \pm 0.26$ and a range of metallicities given by $[8.04, 8.85]$ for their sample of LINERs. While their median value is consistent with the values we report in this work for the differ-

ent grids of photoionization models, both considering AGN or pAGB sources and for both types of LINERs (wAGNs and RGs). However, obtained that we were not able to retrieve oxygen abundances below $12+\log(\text{O/H}) < 8.2$ by means of AGN models, which might be explained by the higher spatial resolution in the Palomar Spectroscopic Survey. In the case of $\log(\text{N/O})$ their findings are also in agreement with those provided by Oliveira et al. (2024b), as well as ours, although the median value that we obtain when considering AGN models is slightly lower ($\log(\text{N/O}) \sim -0.80$).

5.2. Relationships between the nuclear chemical abundances and the host galaxy properties

The relation between $12+\log(\text{O/H})$ and $\log(\text{N/O})$ that we obtained that we obtain for our sample of LINERs in MaNGA is a result that merits a thorough examination given the connotations that this relation has for the evolution of galaxies and the processes driving their chemical enrichment. Our findings are well illustrated in Fig. 5 for different scenarios as a function of the SED considered by the models to calculate the abundances:

- **Strong negative trend:** When pAGB models are accounted for, we obtained a strong anti-correlation between $\log(\text{N/O})$ and $12+\log(\text{O/H})$. When pAGB models with effective tem-

Table 4. Results for the Pearson coefficient correlation test between $\log(\text{N/O})$ and $12+\log(\text{O/H})$ (assuming as null hypothesis that there is no correlation).

Model (1)	Class. (2)	ρ_{Pear} (3)	p-value (4)
AGN $\alpha_{OX} = -0.8$	wAGN	-0.111572	0.408650
	RG	-0.196387	0.180956
	All	-0.175399	0.073503
AGN $\alpha_{OX} = -1.0$	wAGN	-0.526893	0.000025
	RG	-0.294983	0.041814
	All	-0.427234	0.000005
AGN $\alpha_{OX} = -1.2$	wAGN	0.294352	0.026245
	RG	0.321981	0.025631
	All	0.313398	0.001133
AGN $\alpha_{OX} = -1.4$	wAGN	-0.487242	0.000121
	RG	-0.419451	0.003001
	All	-0.482328	0.000000
AGN $\alpha_{OX} = -1.6$	wAGN	-0.568648	0.000004
	RG	-0.377912	0.008091
	All	-0.486132	0.000000
AGN $\alpha_{OX} = -1.8$	wAGN	-0.572961	0.000003
	RG	-0.474195	0.000662
	All	-0.535446	0.000000
AGN $\alpha_{OX} = -2.0$	wAGN	-0.479811	0.000159
	RG	-0.437627	0.001867
	All	-0.477085	0.000000
pAGB $T_{eff} = 5e^4$ K	wAGN	-0.176009	0.190313
	RG	-0.047178	0.750168
	All	-0.139873	0.154701
pAGB $T_{eff} = 1e^5$ K	wAGN	-0.669445	0.000000
	RG	-0.548444	0.000054
	All	-0.620041	0.000000
pAGB $T_{eff} = 1.5e^5$ K	wAGN	-0.656832	0.000000
	RG	-0.757362	0.000000
	All	-0.707616	0.000000
ADAF	wAGN	-0.066046	0.625464
	RG	0.156851	0.287032
	All	-0.006464	0.947821

Notes. For each photoionization model (1) and each group of LINERs (2) the Pearson statistic (3) and the p-value (4) are provided.

perature $T_{eff} = 1 \cdot 10^5$ K are considered, the Pearson correlation coefficients obtained are -0.54 for RGs and -0.67 for wAGNs. In the case of $T_{eff} = 1.5 \cdot 10^5$ K, the coefficients change to -0.75 and -0.65 respectively. In both cases, the anti-correlation spans beyond the limits of the scatter found in the literature.

- **Positive trend:** Only retrieved if an AGN model with slope $\alpha_{OX} = -1.2$ is considered (Pearson correlation coefficients are 0.32 and 0.29 for RGs and wAGNs respectively).
- **Slightly negative trend compatible with the scatter:** For the rest of AGN models, we found negative Pearson correlation coefficients in the range [-0.42, -0.19] for RGs and [-0.53, -0.17] for wAGNs. In all this scenarios, the position in the N/O vs O/H diagram is still compatible with the different relations reported in the literature accounting for the scatter.
- **Nonexistent trend:** Very close to zero Pearson correlation coefficients (0.105 and -0.06 for RGs and wAGNs respectively) are found when ADAF model for inefficient accretion is considered.

In a first order approximation, dynamical process affecting the gas-phase ISM (inflows/outflows), the N/O vs O/H relation

should represent the two scenarios of N production: i) the production of N and O mainly from massive stars, which yields a constant $\log(\text{N/O})$ over $12+\log(\text{O/H}) < 8.5$ (Andrews & Martini 2013; Vincenzo et al. 2016); and, ii) an increasing $\log(\text{N/O})$ ratio over $12+\log(\text{O/H}) > 8.5$ (Andrews & Martini 2013; Vincenzo et al. 2016) as a consequence of the non-negligible contribution of N via intermediate massive stars ($4-7M_{\odot}$ Kobayashi et al. 2020) from the CNO cycles in which contributes the oxygen already present in the stars. In this scenario, the delay between nitrogen production and ejection, N enrichment due to Wolf-Rayet stars (e.g. Kobulnicky et al. 1997; López-Sánchez & Esteban 2010), although might be negligible at kpc scales (e.g. Pérez-Montero et al. 2011), as well as the differences in the star formation efficiency (e.g. Mollá et al. 2006) explain the scatter in the relation reported in the literature, which we exemplified here with the relations from Andrews & Martini (2013) and Belfiore et al. (2015). This scenario allows us to explain not only the observed relation for AGN models in the N/O vs O/H diagram, but also the slight deviation of -0.15 dex for our sample of LINERs as compared to other reported fits of the MZR, as it can be observed in Fig. 6, whereas the deviation in the MNOR diagram (see Fig. 7) is higher.

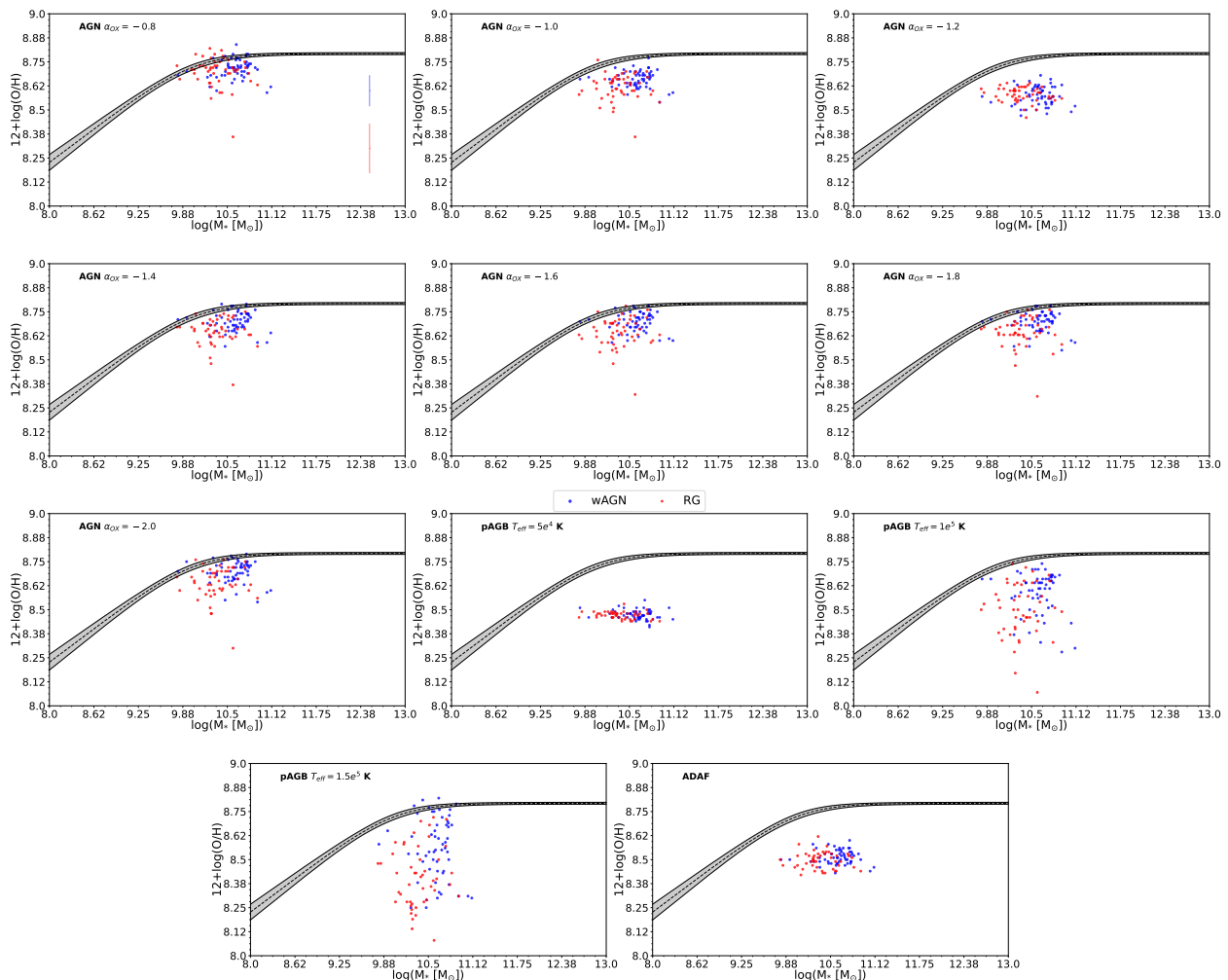


Fig. 6. The mass-metallicity relation (MZR) metallicity determinations in the nuclear regions of our sample of LINERs for different grids of photoionization models. First plot shows the typical errors for the data. Dashed line represent the fit from Curti et al. (2020) and grey-shaded area the corresponding uncertainty on the relation.

Nevertheless, the expected scatter in the O/H vs. N/O relation can be even higher when not considering the galaxy (or the central region) as closed-box model and accounting for gas inflows and outflows as a consequence of stellar evolution or AGN activity. As shown by inflow/outflow chemical evolution models (e.g. Köppen & Edmunds 1999) and supported by observations of interacting systems such as (Ultra)-Luminous Infrared Galaxies (Pérez-Díaz et al. 2024a), the chemical enrichment of Green Pea galaxies (e.g. Amorín et al. 2010, 2012) and specific cases of spatially resolved galaxies such as NGC 4214 (Kobulnicky & Skillman 1996) or NGC 4670 (Kumari et al. 2018). In this case, not only effects on the N production must be taken into account, but also effects on the mixing and gas removal/supply that affects the $12+\log(\text{O}/\text{H})$ abundance ratio. As shown by Pérez-Díaz et al. (2024a), massive infalls of metal-poor gas can drastically dilute $12+\log(\text{O}/\text{H})$ whereas $\log(\text{N}/\text{O})$ remains mostly unaffected during the process, which might explain the high nitrogen-to-oxygen ratios ($\log(\text{N}/\text{O}) > -0.70$) at low oxygen abundances ($12+\log(\text{O}/\text{H}) < 8.4$) observed when pAGB models. In the case of the Teacup nebula, (Villar Martín, M. et al. 2024) showed that outflows might be responsible from a pollution from the central region towards the outer parts, lowering oxygen abundances but keeping high N/O ratios. This result was also found by Oliveira et al. (2024b) when using tailor-made photoionization models

based with pAGB SEDs in their sample of RGs. If this is the scenario, then we should expect a significant scatter in the MZR diagram whereas the MNOR diagram should mimic the behavior for the rest of models. In fact, that is what we obtained for pAGB models.

In order to assess the origin of the observed anti-correlation between O/H and N/O under certain model assumptions, we explored the influence of different galaxy/gas properties, as shown in Fig. 10. For this plot, we took into account estimations for "wAGN" galaxies assuming AGN models while pAGB models ($T_{\text{eff}} = 1 \cdot 10^5 \text{ K}$) for "RG" galaxies. First of all, it is clearly shown that whereas wAGNs do follow the N/O vs O/H relation within the scatter, this is not the case for RGs as they show an anti-correlation that spans beyond the scatter. In panels a) and b) we analyzed whether this relation is driven by physical properties of the gas-phase ISM such as electron density or the ionization parameter. We observed that none of them present a correlation. In panel c) we show the anti-correlation as a function of the stellar mass, finding again no relation at all. In panel d) we show the HI mass reported for each galaxy. From this panel we can extract two conclusions: i) neither the scatter within the reported relation nor the anti-correlation are driven by the amount of gas, as it is observed for the sample of wAGNs; ii) only one of the LINERs classified as RG and with high $\log(\text{N}/\text{O}) (> -0.6)$ and low

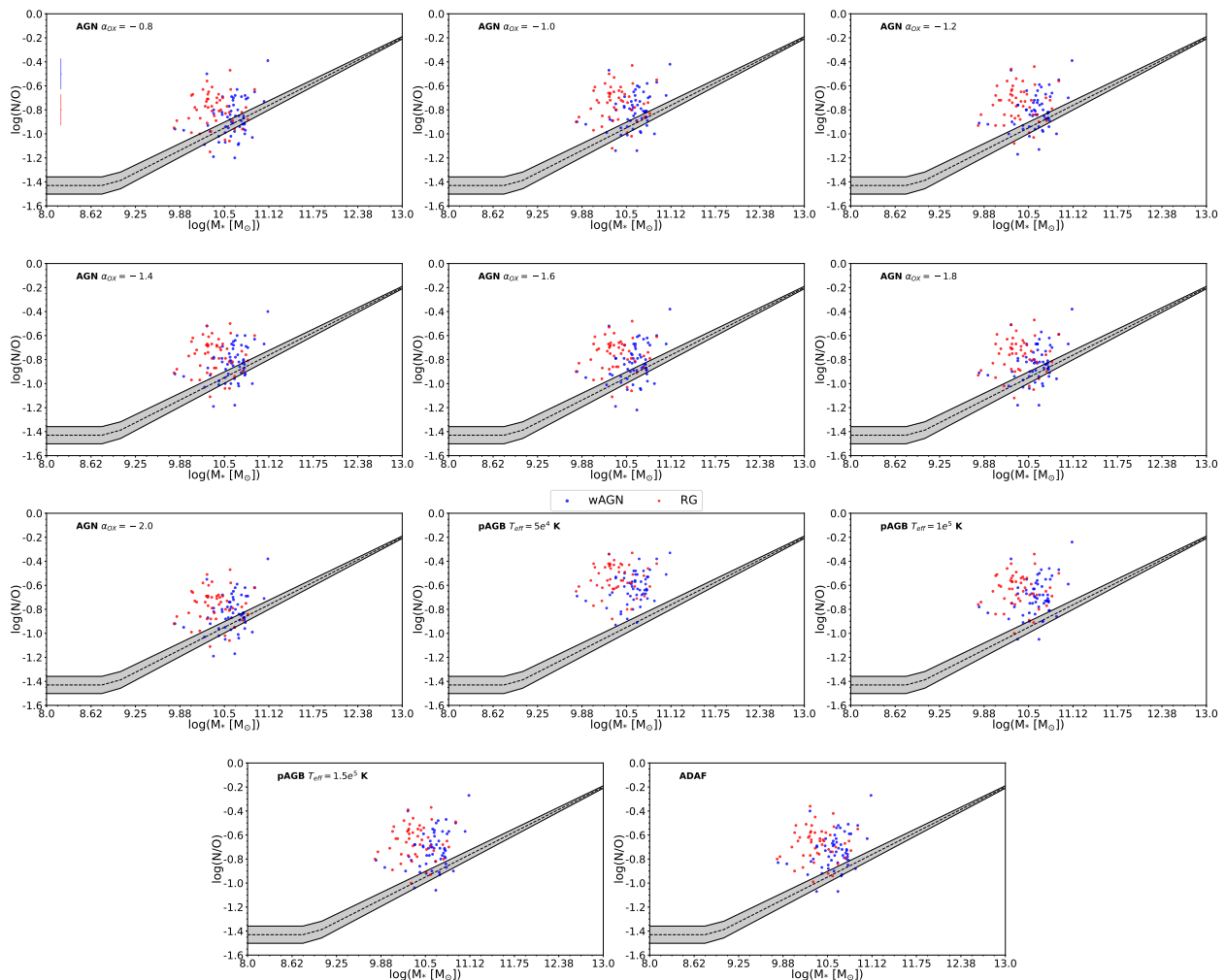


Fig. 7. The mass-NO relation (MNOR) based on the metallicity determinations in the nuclear regions of our sample of LINERs for different grids of photoionization models. First plot shows the typical errors for the data. Dashed line represent the fit from Andrews & Martini (2013) and grey-shaded area the corresponding uncertainty on the relation.

$12+\log(\text{O}/\text{H}) < 8.25$) presents slightly higher gas content than the rest of the sample. However, due to the lack of measurements for most of them, it is not possible to assess whether this object is an outlier or not. Finally, in panel e) we represent the equivalent width of $\text{H}\alpha$. Considering these results, we can explore the inflows and/or outflows scenarios for the anti-correlation.

If the inflow of gas is the major driver of the observed relation, we found several caveats. The first one is the origin of the gas. In the case of Green Pea galaxies, impact with metal-poor high velocity clouds (HVCs, e.g. Köppen & Hensler 2005) or gas accretion from the Cosmic Web (Sánchez Almeida et al. 2015) have been proposed. In the case reported by Pérez-Díaz et al. (2024a), gas is driven by merger interaction, and the amount of gas to dilute the metallicity from $12+\log(\text{O}/\text{H}) = 8.7$ (solar) to $12+\log(\text{O}/\text{H}) = 8.1$ can be expected from the reservoirs of gas from the own galaxy as well as tidal gas taken from the companion (e.g. Montuori et al. 2010; Rupke et al. 2010; Sparre et al. 2022). Considering that the anti-correlation holds in RGs assumed to be populated by pAGB, it is necessary to justify not only the presence of that gas (which is not found when looking at the mass of HI), but also the physical driver towards the nuclear region of those galaxies. The second caveat is also related to the first one, which is the chemical composition of the inflowing gas. To dilute the oxygen content more than 0.5 dex, metal-poor gas

is required, and gas flows from the outer parts to the inner parts, an almost flattened gradient is expected, or if the timescale of the gas dynamics is large enough, a positive gradient from the center to the outer parts. This scenario and its implications is explored in the second paper of these series. The third caveat is the consequences of that inflowing gas. Due to the amount of gas required, and as reported by Pérez-Díaz et al. (2024a) in (U)LIRGs as well as in simulations (Montuori et al. 2010), an increase in the star-formation rate would be expected and, hence, the equivalent width of $\text{H}\alpha$ should be higher (Cid Fernandes et al. 2010) for the most extreme cases, which implies that those would have never been classified as RGs. Moreover, there is no trend in increasing equivalent width of $\text{H}\alpha$, as seen in Fig. 10 panel e).

On the other hand, when considering the outflow scenario as the major driver of this relation some caveats arise. The first one is that observational results for a sample of LINERs classified as RGs presented by Oliveira et al. (2024b) show no evidence of disturbed kinematics in the gas, as it would be expected from the outflow scenario. Another caveat arises in the metallicity gradient: outflow would carry gas until some distance depending on its power and, thus, a change in the metallicity gradient for both $12+\log(\text{O}/\text{H})$ and $\log(\text{N}/\text{O})$ should be expected, with a change in the slope of the gradient at some point as a consequence of the additional enrichment, as it is the case in AGN powered-

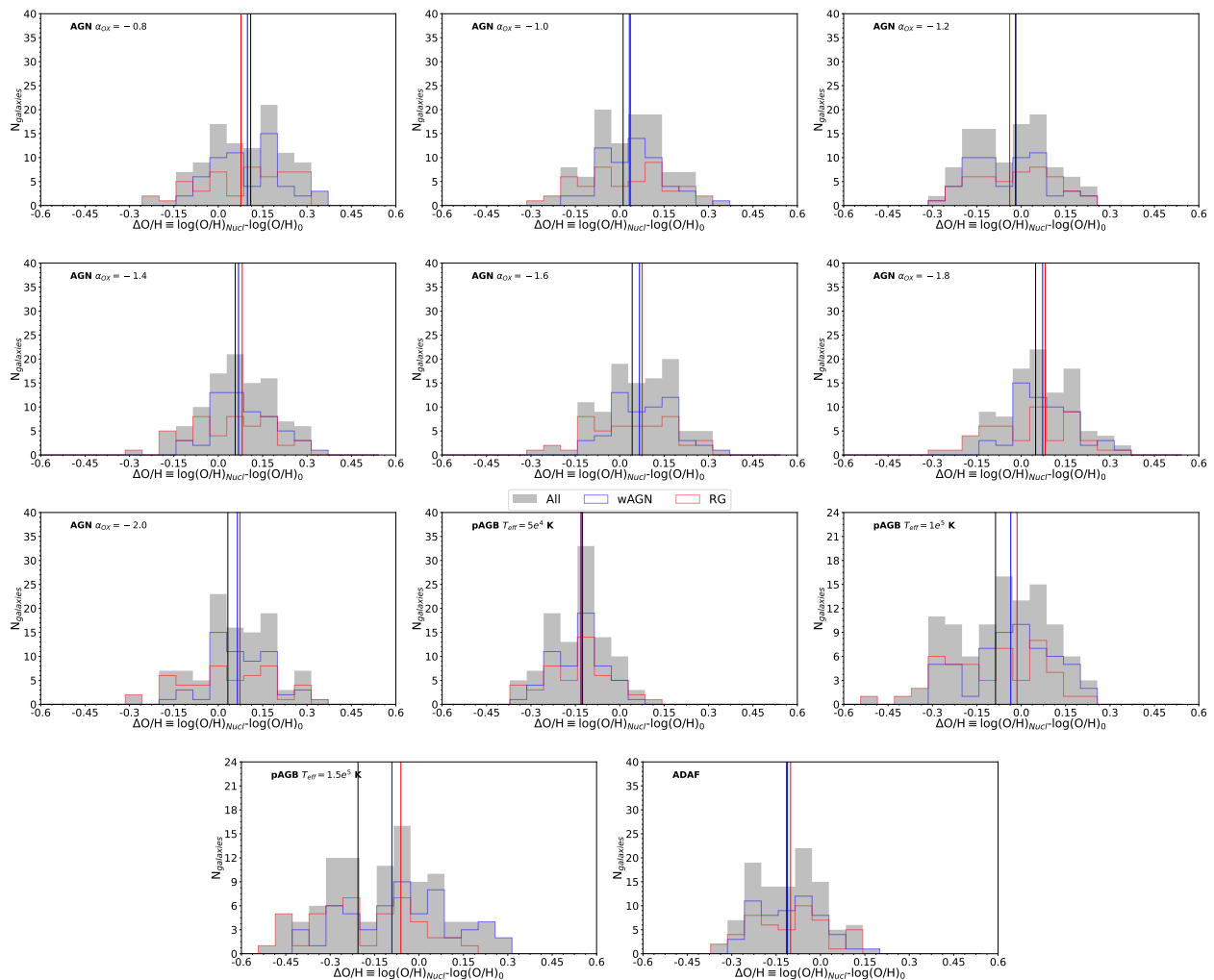


Fig. 8. Histograms of the difference between $12+\log(\text{O}/\text{H})_{\text{Nuc}}$ as estimated in the central regions using different photoionization models and $12+\log(\text{O}/\text{H})_0$ as extrapolated from metallicity gradients. Step-filled grey histogram corresponds to all LINERs in our sample. Step blue and red histograms correspond to wAGNs and RGs respectively. Vertical solid lines represent the median values for each distribution.

outflows (e.g. Villar Martín, M. et al. 2024). Although we will explore this scenario in the next paper, we already have some hints. If outflows are polluting the ISM at galactic scales, then the increase in $\log(\text{N}/\text{O})$ would translate into an overestimation of the $\log(\text{N}/\text{O})$ extrapolated to the nuclear region and, contrary to this idea, we find in Fig. 9 an excellent agreement between the nuclear estimation and nuclear extrapolation. Finally, if outflows are indeed present in sources assumed to be ionized by pAGB, the most likely scenario is that those systems of pAGB stars are driving the outflows and, since they are required to be ionizing the whole nuclear region, the gas would account for an additional contribution of shock emission, thus assuming just purely pAGB models will be inappropriate to model the ionizing structure.

Although we cannot totally exclude a inflowing/outflowing scenario capable to explain the observed anti-correlation between $12+\log(\text{O}/\text{H})$ and $\log(\text{N}/\text{O})$ when it is assumed that pAGB stars are responsible for the emission on some LINERs, we must bear in mind the numerous caveats that those scenarios imply, and that should be carefully revised in future works. We also highlight that this is not a problem if all LINERs are considered to be hosting AGNs, as the anti-correlation is much weaker and compatible with the scatter in the relation as reported in the literature.

5.3. On the source of ionization

The nature of the source of the gas ionization in LINER-like galaxies is still an open question (e.g. Binette et al. 1994; Kewley et al. 2006; Nemmen et al. 2014). Among the different scenarios proposed to explore the origin of ionization of the nuclear gas-phase ISM in LINERs, we explored three scenarios: i) standard AGN models with different SEDs shapes; ii) pAGB stars; and, iii) inefficient accretion leading to an ADAF regime. With the exception of shocks, which were omitted from this study due to the large number of free parameters required to modelize such emission (e.g. Sutherland & Dopita 2017), all of them comprehend the scenarios proposed to explain such emission.

One of the major caveats or the identification of LINERs from their optical emission lines arises in its possible classification from the diagnostic diagrams. Due to the uncertainty in the classification by the BPT diagrams (Baldwin et al. 1981; Kauffmann et al. 2003; Kewley et al. 2006), Cid Fernandes et al. (2010) proposed an alternative version using the information from the equivalent width of $\text{H}\alpha$ to distinguish between AGNs and retired galaxies. To demonstrate the caveats of distinguishing wAGNs and RGs, we have built a semi-empirical galaxy grid, by re-scaling the $W\text{H}\alpha$ predictions from our grids of photoionization models to the observed Balmer lines and continua

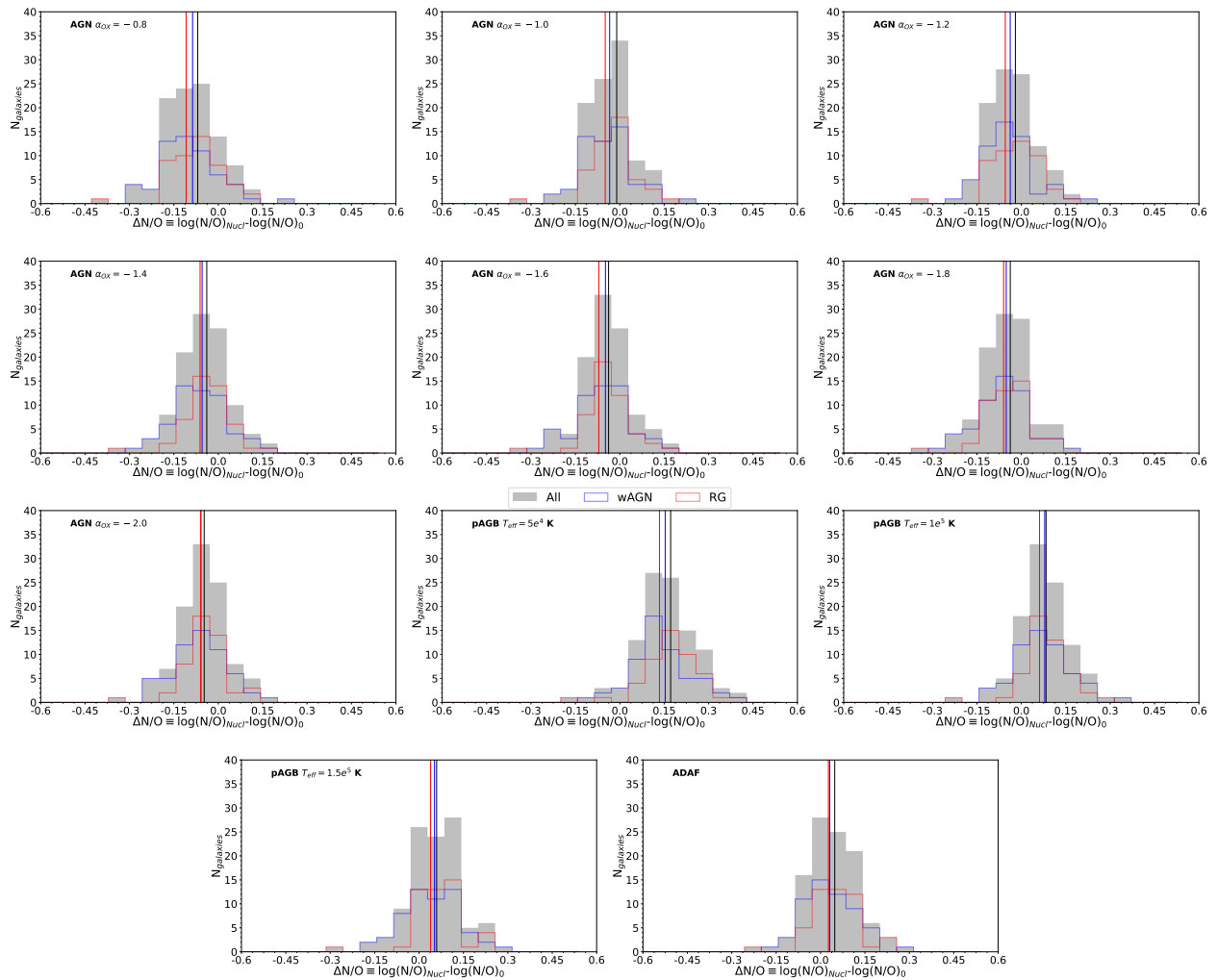


Fig. 9. Same as Fig. 8 but for the difference $\log(N/O)$ as estimated in the central regions using different photoionization models and $\log(N/O)_0$ as extrapolated from metallicity gradients.

in the central spaxels. We then retrieve the expected position on the WHAN diagram for our semi-empirical modeled galaxies based on different properties of the gas-phase ISM ($\log(N/O)$ and $\log(U)$) consistently. As we show in Fig. 11, the position of a galaxy in the WHAN diagram is better provided by a particular combination of $\log(N/O)$ (which allows movement in the X-axis) and $\log(U)$ (allowing changes in the equivalent width) rather than by the ionizing source, although there are differences between the different ionizing sources, but they are not as extreme as to provide a clear classification.

Our study of the chemical abundances in the gas-phase ISM in our selected sample revealed some interesting constraints when different SEDs based on these assumptions were considered in the models. First of all, pAGB models are required to have high effective temperatures ($T_{eff} \geq 1 \cdot 10^5$ K) so as to reproduce the observed properties (Krabbe et al. 2021) as well as to obtain reasonable estimations of the oxygen abundance consistent with other galactic properties, as found in this work. ADAF models, simulating an ionizing SED produced by inefficient accretion (e.g. Nemmen et al. 2014), are not valid to find LINERs out of the range of $8.4 < 12 + \log(O/H) < 8.6$, contrary to the rest of models explored in our work as well as previous studies (Pérez-Díaz et al. 2021; Oliveira et al. 2022, 2024b).

The remaining two scenarios, pAGB stars or AGN standard activity show slight differences on the estimated oxygen content

estimated. The former provides wider ranges and a lower median value ($12 + \log(O/H) = 8.50-8.57$) than the latter ($12 + \log(O/H) = 8.68-8.72$), although the differences are still compatible within the dispersion observed in our sample. As our sample is composed, according to the WHAN diagram, of wAGNs and RGs in a similar proportion (54.3% and 45.7% respectively), it could be expected that the pAGB scenario is favored in RGs whereas the AGN is more accurate for wAGNs. However, we did not find such evidence. On the contrary, by looking at the position of RGs in the MZR (see Fig. 6), if pAGB stars are the source of ionization, then there is an offset of more than 0.5 dex from the expected value of $12 + \log(O/H)$ according to their stellar mass. Moreover, if we account for the secular evolution within the galaxy, we obtain a higher offset between the oxygen abundance as calculated assuming pAGB models and the values extrapolated from the gradient, even in the case of LINERs classified as RGs.

Focusing our attention on the pAGB scenario, we came up with an additional problem. If we consider that pAGB stars emit, on average, $5 \cdot 10^{46}$ ionizing photons per second (Valluri & Anupama 1996), and the average H_α luminosity in the integrated nuclear ($r = 1$ kpc) region is $\log(L(H_\alpha))$ [erg/s] = 39.35 (e.g. Krabbe et al. 2021), we can make use of the relation between the number of ionizing photons and the expected H_α luminosity (Osterbrock

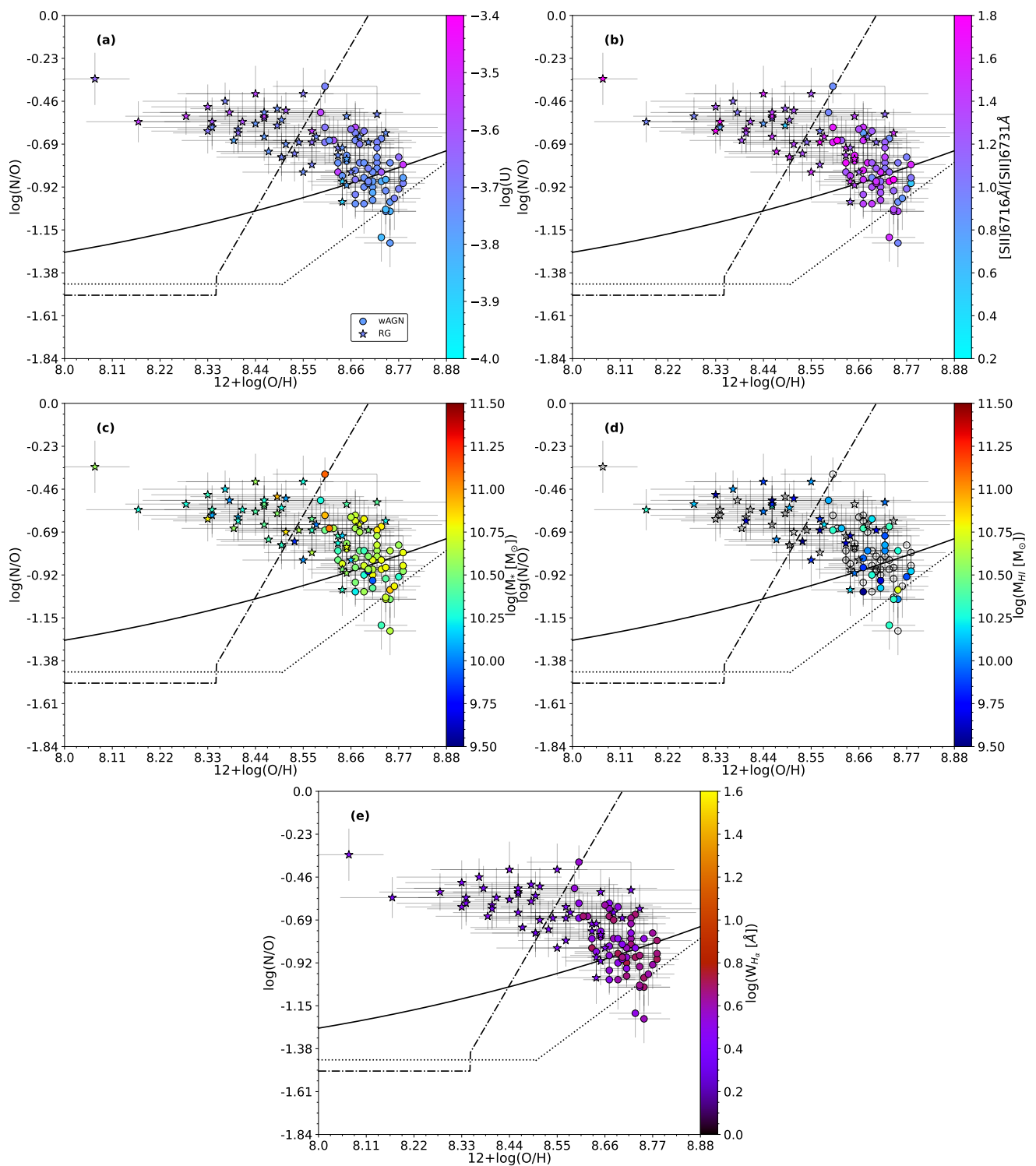


Fig. 10. $\log(N/O)$ vs $12+\log(O/H)$ diagram for our sample of LINERs. Dots represent galaxies classified as "wAGN" and the chemical abundances selected correspond to AGN models with $\alpha_{OX} = -1.6$. Stars correspond to galaxies classified as "RG" whose chemical abundances were estimated assuming pAGB models with $T_{eff} = 1 \cdot 10^5$ K. Colobar show different properties: a) ionization parameter as estimated from emission lines; b) the sulfur ratio tracer of electron density; c) the stellar mass as retrieved from NSA catalogue; d) the HI mass as retrieved from NSA catalogue; and, e) the equivalent width of H_α . Empty forms on the plots correspond to galaxies with no measurement of the represented property.

& Ferland 2006) given by:

$$N_{ion, ph}[s^{-1}] \approx 7.31 \cdot 10^{11} L(H_\alpha) [erg \cdot s^{-1}]$$

which can be used to estimate, assuming ionization bounded conditions, the number of pAGB stars needed to reproduced that

central emission:

$$(1) \quad N_{pAGB} = \frac{N_{ion, ph, tot}}{N_{ion, ph, pAGB}} \approx 1.463 \cdot 10^{-35} L(H_\alpha) [erg \cdot s^{-1}] \quad (2)$$

which in this particular case yields to $3.2 \cdot 10^4$ stars, within a radius of 1 kpc. If all those stars are ionizing the gas nowadays,

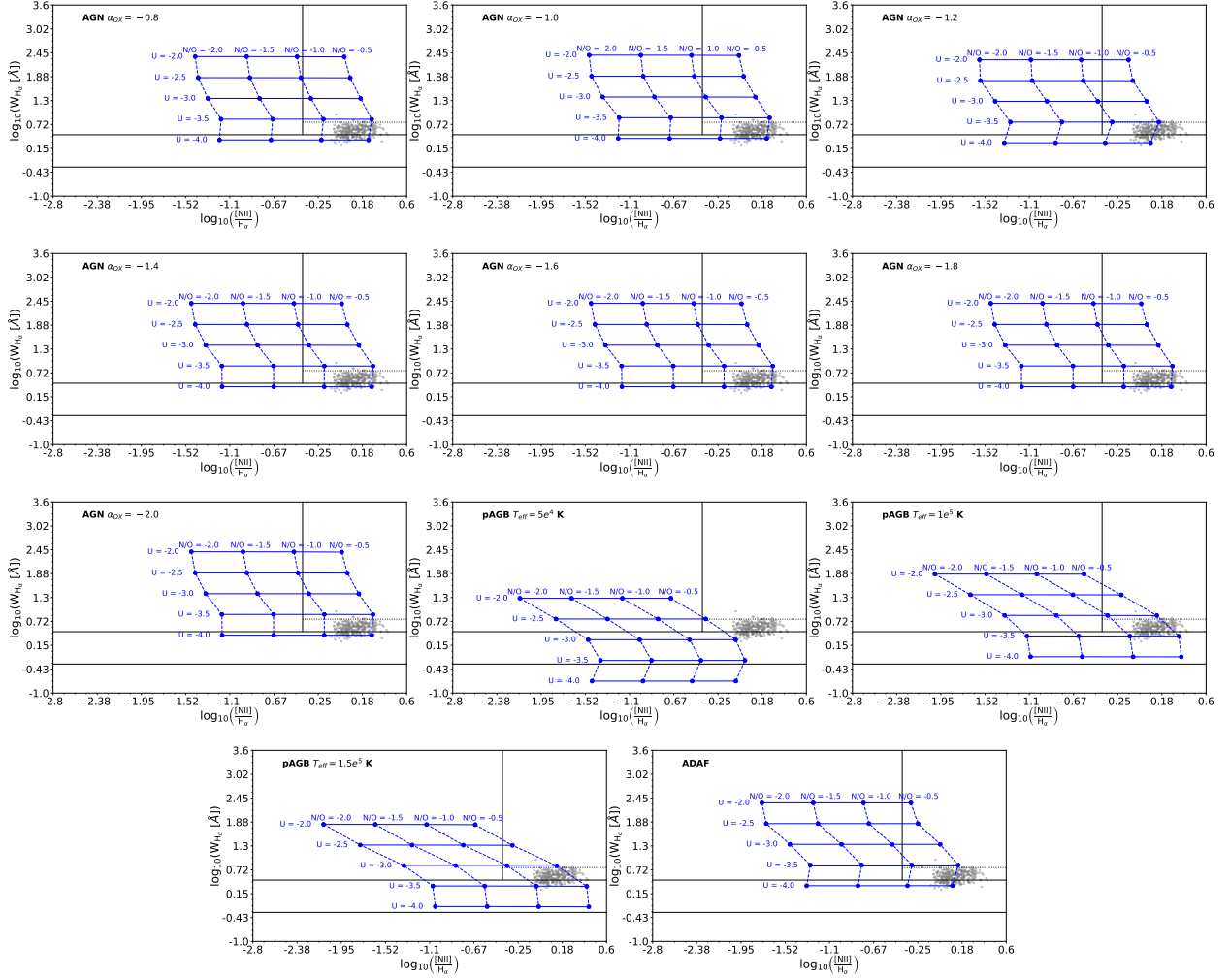


Fig. 11. The WHAN diagram for the LINER-like nuclear regions in our sample (grey dots) showing the coverage of the different grids of photoionization models considered in this work. The grid of models was obtained by limiting the oxygen abundance to $12 + \log(\text{O}/\text{H}) = 8.6$ and employing different values of the ionization parameter $\log(U)$ as well as the nitrogen-to-oxygen abundance ratios $\log(\text{N}/\text{O})$.

we can assume that they were formed roughly at the same time. Assuming the initial mass function (IMF) form from Salpeter (1955), we can then obtain the expected number of stars in a range of mass as:

$$N = \int_{M_{\min}}^{M_{\max}} \xi(M) dM = \int_{M_{\min}}^{M_{\max}} \xi_0 M^{-2.35} dM \quad (3)$$

Considering the expected mass of the progenitors of pAGB stars ranges in $[1.5M_{\odot}, 8M_{\odot}]$ (e.g. Ventura et al. 2017), then we obtain and that the validity of Salpeter's IMF has a minimum value of $0.5M_{\odot}$ and that we will only consider an upper limit of $20M_{\odot}$ (quite conservative), the probability of finding 1 pAGB star can be calculated as:

$$p = \frac{\int_{1.5M_{\odot}}^{8M_{\odot}} \xi_0 M^{-2.35} dM}{\int_{0.5M_{\odot}}^{20M_{\odot}} \xi_0 M^{-2.35} dM} \quad (4)$$

which gives 20.46%, which is consistent with that idea that per globular cluster ($\sim 10^5 L_{\odot}$) one pAGB star is expected (Renzini & Buzzoni 1986; Valluri & Anupama 1996). Notice that this is an upper limit to the probability of finding a pAGB star. Thus, the minimum number of globular clusters expected within 1 kpc radius should be around $\sim 3.2 \cdot 10^4$. For comparison, the number

of globular clusters reported in the inner part of the Milky Way ($r < 3.5$ kpc) is less than 100 (Bica et al. 2024). Thus, the pAGB nature of the ionizing source is less favored.

Overall, conclusiveness on the source of ionization cannot be achieved without other spectral regimes. If the AGN scenario is considered, X-ray counterparts from the accretion disk surrounding the Super Massive Black Hole (SMBH) must be expected. In fact, this is the approach that Pérez-Díaz et al. (2021) followed to justify the assumption of AGN activity when analyzing their sample of LINERs from the Palomar Spectroscopic Survey. Additional constraints can be obtained with X-ray data such as, the shape (α_{OX}) of the SED. Another important constraint can be found on the use of infrared (IR) emission lines, which trace high-ionic species such as O^{++} , O^{3+} , Ne^{++} , Ne^{4+} , Ne^{5+} , Ar^{++} , Ar^{4+} or Ar^{5+} (Pérez-Díaz et al. 2022, 2024b) they might provide SED constraints by means of diagnostic diagrams such as the softness diagram (e.g. Pérez-Montero et al. 2024). We cannot exclude the possibility that pAGB stars ($T_{\text{eff}} \geq 1 \cdot 10^5$ K) are contributing to the ionization of the gas-phase ISM together with central AGN emission, although exploring the exact combination of both ionizing sources would be a much more complex issue for which better constraints are needed.

5.4. N/O as a unbiased tracer of chemical enrichment

Through this study we have made a distinction between LINERs classified as wAGNs and RGs as a consequence of the uncertainty in the nature of the ionizing source in these objects (e.g. Márquez et al. 2017). For this reason, we explored different ionizing scenarios. On one hand, we obtained different $12+\log(\text{O}/\text{H})$ estimations if we account for the AGN or the pAGB scenario (see Table 2 and Fig. 8). On the contrary, an almost negligible change (considering the uncertainties) is found for the estimation of $\log(\text{N}/\text{O})$ for all the assumed SEDs.

The importance of estimating $\log(\text{N}/\text{O})$ was already highlighted by several authors (e.g. Pérez-Montero & Contini 2009; Vincenzo et al. 2016; Pérez-Díaz et al. 2022). First of all, its importance relies on the use of estimators of the oxygen abundance based on N emission lines, as an independent constrain on $\log(\text{N}/\text{O})$ is needed to avoid effects of enhancing metallicity due to high $\log(\text{N}/\text{O})$ ratios (see for instance the difference between Oliveira et al. 2022 and Oliveira et al. 2024b). Secondly, an estimation of N/O complements the information not only, but also on the degree of chemical enrichment (e.g. Pilyugin et al. 2004; Pérez-Montero et al. 2013, 2016; Vincenzo et al. 2016). Thirdly, it remains mostly unaffected by gas dynamics that can alter the chemical composition as traced by $12+\log(\text{O}/\text{H})$ (e.g. Edmunds 1990; Amorín et al. 2010, 2012; Köppen & Hensler 2005; Sánchez Almeida et al. 2015; Pérez-Díaz et al. 2024a).

In addition, from this study on the use of optical emission lines to estimate chemical abundances, we can also add another advantage to the use of $\log(\text{N}/\text{O})$ which is the fact that can be properly estimated without a bias due the assumption of a particular ionizing source. Regardless of the ionizing source assumed for the gas-phase ISM, $\log(\text{N}/\text{O})$ abundances in our sample of LINERs are in the range $[-1.20, -0.27]$, clustering around the value of ~ -0.79 (slightly suprasolar).

6. Conclusions

We have analyzed a sample of 105 optically selected LINERs from SDSS-IV MaNGA. Particularly, we have studied the chemical abundances using photoionization models in their nuclear region accounting for different scenarios representing the uncertainty in the source of ionization: AGN models with different shapes, pAGB models with different effective temperatures and, inefficient accretion AGN models in which the accretion disk is truncated (ADAF). To assess whether one or multiple scenarios might be feasible, we also used the WHAN diagram to discriminate between galaxies with intermediate equivalent widths of $H\alpha$, expected to be weak AGNs (wAGNs), and galaxies with low equivalent widths which are though to be retired galaxies (RGs) and, thus powered by hot-old stellar populations.

Our results show that oxygen abundances ($12+\log(\text{O}/\text{H})$) in the nuclear region of LINERs, with independence on the subtype (wAGN or RG) and the SED considered, spread over a wide range of values: $8.08 \leq 12+\log(\text{O}/\text{H}) \leq 8.82$ in the pAGB scenario, and $8.30 \leq 12+\log(\text{O}/\text{H}) \leq 8.84$ for the AGN scenario. The corresponding median value is $12+\log(\text{O}/\text{H}) = 8.69$ (solar) for the AGN scenario, whereas it drops to $12+\log(\text{O}/\text{H}) = 8.53$ (slightly subsolar) in the pAGB scenario. The nitrogen-to-oxygen abundance ratios ($\log(\text{N}/\text{O})$) are mainly suprasolar, within the range $-1.20 \leq \log(\text{N}/\text{O}) \leq -0.38$ (if AGNs are considered) or $-1.07 \leq \log(\text{N}/\text{O}) \leq -0.27$. The median value reported in the pAGB scenario is slightly higher ($\log(\text{N}/\text{O}) = -0.69$) than in the AGN scenario ($\log(\text{N}/\text{O}) = -0.79$), in both cases slightly suprasolar. Overall, LINERs are characterized mainly by supra-

solar $\log(\text{N}/\text{O})$ ratios and sub- or close-to solar $12+\log(\text{O}/\text{H})$ ratios. When analyzing the behavior of these nuclear estimations with host galaxy physical properties, such as stellar mass, no correlation is found, and we report a scatter in the MNOR diagram rather than in the MZR diagram.

The assumptions on the nature of the ionizing source are more critical when analyzing the $12+\log(\text{O}/\text{H})$ as pAGB models, introducing much more scatter in the MZR relation as well as in their comparison with the extrapolation from metallicity gradients. This is highlighted when looking at the behavior on the $\log(\text{N}/\text{O})$ vs $12+\log(\text{O}/\text{H})$. If LINERs are considered to be powered by AGNs, little correlation is found between both quantities, but the data fits in the scatter of the reported relation in the literature. On the contrary, if LINERs are considered to be powered by pAGB stars, then a negative correlation is found between both quantities, as previously reported in the literature. We discussed several scenarios to explain such anti-correlation, although more specific studies on this result must be performed in order to obtain more robust conclusions.

Although we cannot rule out the possibility that emission in LINERs might be explained from pAGB stars, our study reveals that several problems arise from this assumption. First of all, in order to reproduce the emission detected in the nuclear region a large number of pAGB stars is required, which is hard to explain both the number and its co-existence. Secondly, the results on the chemical enrichment (as seen from $\log(\text{N}/\text{O})$ vs $12+\log(\text{O}/\text{H})$ diagram) points towards a complex scenario in which extreme events are needed to explain the observed relation. On the contrary, if LINERs are assumed to be powered by AGNs, the chemical enrichment scenario, in general, does not depart from the reported trends in the literature although some hints on anti-correlation are found which might be explained with the scatter caused by the delay on the N production as well as other gas dynamical effects affecting $12+\log(\text{O}/\text{H})$, but less extreme than in the pAGB scenario.

Data availability

Tables B.1–B.5 are available in electronic form at the CDS via anonymous ftp to cdsarc.u-strasbg.fr (130.79.128.5) or via <http://cdsweb.u-strasbg.fr/cgi-bin/qcat?J/A+A/>.

Acknowledgements. We acknowledge support from the Spanish MINECO grant PID2022-136598NB-C32. We acknowledge financial support from the Severo Ochoa grant CEX2021-001131-S MICIU/AEI/10.13039/501100011033. This research made use of ASTROPY, which is a community-developed core Python package for Astronomy (Astropy Collaboration et al. 2013, 2018, 2022), and other software and packages: NUMPY (van der Walt et al. 2011), and SCIPY (Virtanen et al. 2020). The plots for this research were created using MATPLOTLIB (Hunter 2007). We acknowledge the fruitful discussions with our research team. We thank the anonymous referee for the constructive report that improved this manuscript. E.P.M. acknowledges the assistance from his guide dog, Rocko, without whose daily help this work would have been much more difficult.

References

- Abdurro'uf, Accetta, K., Aerts, C., et al. 2022, ApJS, 259, 35
- Allen, M. G., Groves, B. A., Dopita, M. A., Sutherland, R. S., & Kewley, L. J. 2008, ApJS, 178, 20
- Amorín, R., Pérez-Montero, E., Vílchez, J. M., & Papaderos, P. 2012, ApJ, 749, 185
- Amorín, R. O., Pérez-Montero, E., & Vílchez, J. M. 2010, ApJ, 715, L128
- Andrews, B. H. & Martini, P. 2013, ApJ, 765, 140
- Annibali, F., Bressan, A., Rampazzo, R., et al. 2010, A&A, 519, A40
- Asari, N. V., Cid Fernandes, R., Stasińska, G., et al. 2007, MNRAS, 381, 263
- Asplund, M., Grevesse, N., Sauval, A. J., & Scott, P. 2009, ARA&A, 47, 481
- Astropy Collaboration, Price-Whelan, A. M., Lim, P. L., et al. 2022, ApJ, 935, 167

- Astropy Collaboration, Price-Whelan, A. M., Sipőcz, B. M., et al. 2018, *AJ*, 156, 123
- Astropy Collaboration, Robitaille, T. P., Tollerud, E. J., et al. 2013, *A&A*, 558, A33
- Baldwin, J. A., Phillips, M. M., & Terlevich, R. 1981, *PASP*, 93, 5
- Belfiore, F., Maiolino, R., Bundy, K., et al. 2015, *MNRAS*, 449, 867
- Bennert, N., Jungwiert, B., Komossa, S., Haas, M., & Chini, R. 2006a, *A&A*, 456, 953
- Bennert, N., Jungwiert, B., Komossa, S., Haas, M., & Chini, R. 2006b, *A&A*, 456, 953
- Bica, E., Ortolani, S., Barbuy, B., & Oliveira, R. A. P. 2024, *A&A*, 687, A201
- Binette, L., Magris, C. G., Stasińska, G., & Bruzual, A. G. 1994, *A&A*, 292, 13
- Blanton, M. R., Bershady, M. A., Abolfathi, B., et al. 2017, *AJ*, 154, 28
- Bruzual, G. & Charlot, S. 2003, *MNRAS*, 344, 1000
- Bundy, K., Bershady, M. A., Law, D. R., et al. 2015, *ApJ*, 798, 7
- Capelo, P. R., Feruglio, C., Hickox, R. C., & Tombesi, F. 2023, in *Handbook of X-ray and Gamma-ray Astrophysics*, 126
- Carvalho, S. P., Dors, O. L., Cardaci, M. V., et al. 2020, *MNRAS*, 492, 5675
- Chabrier, G. 2003, *ApJ*, 586, L133
- Cid Fernandes, R., Mateus, A., Sodré, L., Stasińska, G., & Gomes, J. M. 2005, *MNRAS*, 358, 363
- Cid Fernandes, R., Stasińska, G., Mateus, A., & Vale Asari, N. 2011, *MNRAS*, 413, 1687
- Cid Fernandes, R., Stasińska, G., Schlickmann, M. S., et al. 2010, *MNRAS*, 403, 1036
- Contini, M. & Aldrovandi, S. M. V. 1983, *A&A*, 127, 15
- Coziol, R., Reyes, R. E. C., Considère, S., Davoust, E., & Contini, T. 1999, *A&A*, 345, 733
- Curti, M., Mannucci, F., Cresci, G., & Maiolino, R. 2020, *MNRAS*, 491, 944
- Cybart, R. H., Fields, B. D., Olive, K. A., & Yeh, T.-H. 2016, *Reviews of Modern Physics*, 88, 015004
- Davies, R. L., Groves, B., Kewley, L. J., et al. 2016, *MNRAS*, 462, 1616
- de Nicola, S., Marconi, A., & Longo, G. 2019, *MNRAS*, 490, 600
- Dopita, M. A. & Sutherland, R. S. 1995, *ApJ*, 455, 468
- Dors, O. L., Cardaci, M. V., Hägele, G. F., et al. 2015, *MNRAS*, 453, 4102
- Dors, O. L., Valerdi, M., Riffel, R. A., et al. 2023, *MNRAS*, 521, 1969
- Duarte Puertas, S., Vilchez, J. M., Iglesias-Páramo, J., et al. 2022, *A&A*, 666, A186
- Eckert, D., Gaspari, M., Gastaldello, F., Le Brun, A. M. C., & O'Sullivan, E. 2021, *Universe*, 7, 142
- Edmunds, M. G. 1990, *MNRAS*, 246, 678
- Ferland, G. J., Chatzikos, M., Guzmán, F., et al. 2017, *Rev. Mexicana Astron. Astrofis.*, 53, 385
- Fernández-Ontiveros, J. A., Pérez-Montero, E., Vilchez, J. M., Amorín, R., & Spinoglio, L. 2021, *A&A*, 652, A23
- Gaskell, C. M. 2009, *New A Rev.*, 53, 140
- Gitti, M., Brighenti, F., & McNamara, B. R. 2012, *Advances in Astronomy*, 2012, 950641
- Grisoni, V., Matteucci, F., & Romano, D. 2021, *MNRAS*, 508, 719
- Henry, R. B. C., Edmunds, M. G., & Köppen, J. 2000, *ApJ*, 541, 660
- Ho, L. C. 2009, *ApJ*, 699, 626
- Ho, L. C., Filippenko, A. V., & Sargent, W. L. W. 1997, *ApJS*, 112, 315
- Ho, L. C., Shields, J. C., & Filippenko, A. V. 1993, *ApJ*, 410, 567
- Howarth, I. D. 1983, *Monthly Notices of the Royal Astronomical Society*, 203, 301
- Hunter, J. D. 2007, *Computing in Science and Engineering*, 9, 90
- Ilić, D., Shapovalova, A. I., Popović, L. Č., et al. 2017, *Frontiers in Astronomy and Space Sciences*, 4, 12
- Kauffmann, G., Heckman, T. M., Tremonti, C., et al. 2003, *MNRAS*, 346, 1055
- Kewley, L. J., Groves, B., Kauffmann, G., & Heckman, T. 2006, *MNRAS*, 372, 961
- Kobayashi, C., Karakas, A. I., & Lugaro, M. 2020, *ApJ*, 900, 179
- Kobulnicky, H. A., Kennicutt, Robert C., J., & Pizagno, J. L. 1999, *ApJ*, 514, 544
- Kobulnicky, H. A. & Skillman, E. D. 1996, *ApJ*, 471, 211
- Kobulnicky, H. A., Skillman, E. D., Roy, J.-R., Walsh, J. R., & Rosa, M. R. 1997, *ApJ*, 477, 679
- Köppen, J. & Edmunds, M. G. 1999, *MNRAS*, 306, 317
- Köppen, J. & Hensler, G. 2005, *A&A*, 434, 531
- Krabbe, A. C., Oliveira, C. B., Zinchenko, I. A., et al. 2021, *MNRAS*, 505, 2087
- Kumari, N., James, B. L., Irwin, M. J., Amorín, R., & Pérez-Montero, E. 2018, *MNRAS*, 476, 3793
- Law, D. R., Cherinka, B., Yan, R., et al. 2016, *AJ*, 152, 83
- Lequeux, J., Peimbert, M., Rayo, J. F., Serrano, A., & Torres-Peimbert, S. 1979, *A&A*, 500, 145
- López-Sánchez, Á. R. & Esteban, C. 2010, *A&A*, 517, A85
- Maiolino, R. & Mannucci, F. 2019, *A&A Rev.*, 27, 3
- Mandal, A. K., Rakshit, S., Stalin, C. S., et al. 2021, *MNRAS*, 502, 2140
- Marconi, A., Amiri, A., Feltre, A., et al. 2024, *arXiv e-prints*, arXiv:2401.13028
- Márquez, I., Masegosa, J., González-Martin, O., et al. 2017, *Frontiers in Astronomy and Space Sciences*, 4, 34
- Mateus, A., Sodré, L., Cid Fernandes, R., et al. 2006, *MNRAS*, 370, 721
- McClure, R. D. & van den Bergh, S. 1968, *AJ*, 73, 1008
- Méndez-Delgado, J. E., Esteban, C., García-Rojas, J., Kreckel, K., & Peimbert, M. 2023, *Nature*, 618, 249
- Mollá, M., García-Vargas, M. L., & Bressan, A. 2009, *MNRAS*, 398, 451
- Mollá, M., Vilchez, J. M., Gavilán, M., & Díaz, A. I. 2006, *MNRAS*, 372, 1069
- Montuori, M., Di Matteo, P., Lehnert, M. D., Combes, F., & Semelin, B. 2010, *A&A*, 518, A56
- Morganti, R. 2017, *Frontiers in Astronomy and Space Sciences*, 4, 42
- Nemmen, R. S., Storchi-Bergmann, T., & Eracleous, M. 2014, *MNRAS*, 438, 2804
- Nobels, F. S. J., Schaye, J., Schaller, M., Bahé, Y. M., & Chaikin, E. 2022, *MNRAS*, 515, 4838
- Oliveira, C. B., Dors, O. L., Zinchenko, I. A., et al. 2024a, *arXiv e-prints*, arXiv:2411.02043
- Oliveira, C. B., Krabbe, A. C., Dors, O. L., et al. 2024b, *MNRAS*, 531, 199
- Oliveira, C. B., Krabbe, A. C., Hernandez-Jimenez, J. A., et al. 2022, *MNRAS*, 515, 6093
- Osterbrock, D. E. & Ferland, G. J. 2006, *Astrophysics of gaseous nebulae and active galactic nuclei*
- Page, M. J., Stevens, J. A., Ivison, R. J., & Carrera, F. J. 2004, *ApJ*, 611, L85
- Peimbert, M. 1967, *ApJ*, 150, 825
- Peimbert, M. & Costero, R. 1969, *Boletín de los Observatorios Tonantzintla y Tacubaya*, 5, 3
- Peimbert, M., Luridiana, V., & Peimbert, A. 2007, *ApJ*, 666, 636
- Pérez-Díaz, B., Masegosa, J., Márquez, I., & Pérez-Montero, E. 2021, *MNRAS*, 505, 4289
- Pérez-Díaz, B., Pérez-Montero, E., Fernández-Ontiveros, J. A., & Vilchez, J. M. 2022, *A&A*, 666, A115
- Pérez-Díaz, B., Pérez-Montero, E., Fernández-Ontiveros, J. A., Vilchez, J. M., & Amorín, R. 2024a, *Nature Astronomy*, 8, 368
- Pérez-Díaz, B., Pérez-Montero, E., Fernández-Ontiveros, J. A., et al. 2024b, *A&A*, 685, A168
- Pérez-Montero, E. 2014, *MNRAS*, 441, 2663
- Pérez-Montero, E. & Amorín, R. 2017, *MNRAS*, 467, 1287
- Pérez-Montero, E., Amorín, R., Sánchez Almeida, J., et al. 2021, *MNRAS*, 504, 1237
- Pérez-Montero, E. & Contini, T. 2009, *MNRAS*, 398, 949
- Pérez-Montero, E., Contini, T., Lamareille, F., et al. 2013, *A&A*, 549, A25
- Pérez-Montero, E. & Díaz, A. I. 2005, *MNRAS*, 361, 1063
- Pérez-Montero, E., Dors, O. L., Vilchez, J. M., et al. 2019, *MNRAS*, 489, 2652
- Pérez-Montero, E., Fernández-Ontiveros, J. A., Pérez-Díaz, B., et al. 2024, *A&A*, 684, A40
- Pérez-Montero, E., García-Benito, R., Hägele, G. F., & Díaz, Á. I. 2010, *MNRAS*, 404, 2037
- Pérez-Montero, E., García-Benito, R., Vilchez, J. M., et al. 2016, *A&A*, 595, A62
- Pérez-Montero, E., Vilchez, J. M., Cedrés, B., et al. 2011, *A&A*, 532, A141
- Pérez-Montero, E., Zinchenko, I. A., Vilchez, J. M., et al. 2023, *A&A*, 669, A88
- Peterson, B. M. 2006, in *Physics of Active Galactic Nuclei at all Scales*, ed. D. Alloin, Vol. 693, 77
- Peterson, B. M., Denney, K. D., De Rosa, G., et al. 2013, *ApJ*, 779, 109
- Pilyugin, L. S., Vilchez, J. M., & Contini, T. 2004, *A&A*, 425, 849
- Pović, M., Márquez, I., Netzer, H., et al. 2016, *MNRAS*, 462, 2878
- Rauch, T. 2003, *A&A*, 403, 709
- Renzini, A. & Buzzoni, A. 1986, in *Astrophysics and Space Science Library*, Vol. 122, *Spectral Evolution of Galaxies*, ed. C. Chiosi & A. Renzini, 195–231
- Rupke, D. S. N., Kewley, L. J., & Barnes, J. E. 2010, *ApJ*, 710, L156
- Salpeter, E. E. 1955, *ApJ*, 121, 161
- Sánchez Almeida, J., Elmegreen, B. G., Muñoz-Tuñón, C., et al. 2015, *ApJ*, 810, L15
- Sánchez-Menguiano, L., Sánchez Almeida, J., Sánchez, S. F., & Muñoz-Tuñón, C. 2024, *A&A*, 681, A121
- Searle, L. 1971, *ApJ*, 168, 327
- Searle, L. & Sargent, W. L. W. 1972, *ApJ*, 173, 25
- Sharda, P., Ginzburg, O., Krumholz, M. R., et al. 2024, *MNRAS*, 528, 2232
- Sparre, M., Whittingham, J., Damle, M., et al. 2022, *MNRAS*, 509, 2720
- Stasińska, G., Vale Asari, N., Cid Fernandes, R., et al. 2008, *MNRAS*, 391, L29
- Storchi-Bergmann, T., Schmitt, H. R., Calzetti, D., & Kinney, A. L. 1998, *AJ*, 115, 909
- Sutherland, R. S. & Dopita, M. A. 2017, *ApJS*, 229, 34
- Thomas, A. D., Dopita, M. A., Kewley, L. J., et al. 2018, *ApJ*, 856, 89
- Thuan, T. X., Izotov, Y. I., & Lipovetsky, V. A. 1995, *ApJ*, 445, 108
- Tremonti, C. A., Heckman, T. M., Kauffmann, G., et al. 2004, *ApJ*, 613, 898
- Valluri, M. & Anupama, G. C. 1996, *AJ*, 112, 1390
- van der Walt, S., Colbert, S. C., & Varoquaux, G. 2011, *Computing in Science and Engineering*, 13, 22
- Veilleux, S. & Osterbrock, D. E. 1987, *ApJS*, 63, 295

- Ventura, P., Stanghellini, L., Dell’Agli, F., & García-Hernández, D. A. 2017, MNRAS, 471, 4648
- Vila-Costas, M. B. & Edmunds, M. G. 1993, MNRAS, 265, 199
- Vilchez, J. M., Pagel, B. E. J., Diaz, A. I., Terlevich, E., & Edmunds, M. G. 1988, MNRAS, 235, 633
- Villar Martín, M., López Cobá, C., Cazzoli, S., Pérez Montero, E., & Cabrera Lavers, A. 2024, A&A, 690, A397
- Vincenzo, F., Belfiore, F., Maiolino, R., Matteucci, F., & Ventura, P. 2016, MNRAS, 458, 3466
- Virtanen, P., Gommers, R., Oliphant, T. E., et al. 2020, Nature Methods, 17, 261
- Yuan, F., Cui, W., & Narayan, R. 2005, ApJ, 620, 905
- Yuan, F., Zdziarski, A. A., Xue, Y., & Wu, X.-B. 2007, ApJ, 659, 541
- Zinchenko, I. A., Pilyugin, L. S., Grebel, E. K., Sánchez, S. F., & Vilchez, J. M. 2016, MNRAS, 462, 2715
- Zinchenko, I. A., Vilchez, J. M., Pérez-Montero, E., et al. 2021, A&A, 655, A58

Appendix A: Comparison of estimations of chemical abundances

We present in this appendix a global comparison among the chemical abundances estimated in the nuclear region of our sample of LINER-like galaxies based on different assumptions for the ionizing source.

We show in Fig. A.1 the comparison among the oxygen abundances estimated in the nuclear region of our sample of LINER-like galaxies based on different grids of photoionization models. Despite there is a little discrepancy when AGN models with $\alpha_{OX} = -1.2$ are considered, we can conclude that changes in the slope (α_{OX}) of the AGN SED do not induce changes in the estimation of $12+\log(\text{O}/\text{H})$. In the same way, very little change is found when switching from pAGB models characterized by $T_{eff} = 1 \cdot 10^5$ K to $T_{eff} = 1.5 \cdot 10^5$ K. When comparing AGN models and pAGB models, we observed that from $12+\log(\text{O}/\text{H}) = 8.1$ to $12+\log(\text{O}/\text{H}) = 8.7$ (solar value), pAGB models predict systematically lower chemical abundances than AGN models. Fig. A.1 also highlights the problem of assuming pAGB models with low effective temperatures ($T_{eff} = 5 \cdot 10^4$ K).

On the contrary, Fig. A.2 shows the excellent agreement among the estimations of $\log(\text{N}/\text{O})$. Omitting pAGB models characterized by $T_{eff} = 5 \cdot 10^4$ K, which have been already probed to be inappropriate for this analysis, there is correlation one-to-one for all photoionization models considered. We also noticed that there is a small offset between AGN models and ADAF or pAGB models, although the correlation one-to-one still holds.

Appendix B: Data

We present in this appendix the full dataset used for this work. Table B.1 contains all ancillary data for our sample of galaxies. Table B.2 lists all optical spectroscopic properties of the nuclear regions of our sample of LINER-like galaxies. Tables B.3 - B.5 list all the estimations of chemical abundances and ionization parameters for the nuclear regions of our sample.

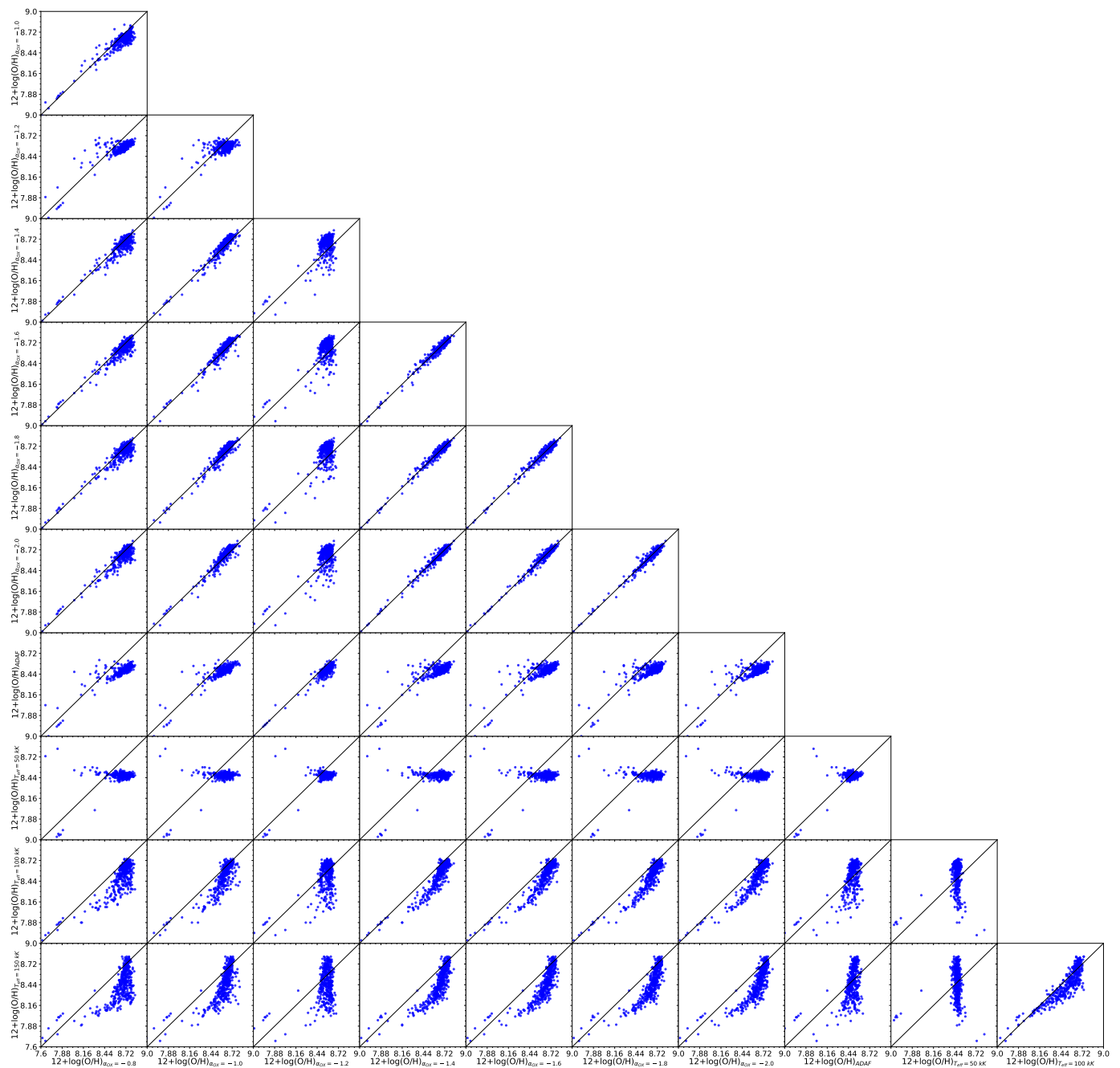


Fig. A.1. Comparative plot of oxygen abundances in the nuclear regions of our sample of LINERs for each grid of photoionization models considered in this work.

Table B.1. List of galaxies and host galaxy properties in our sample of LINER-like galaxies.

MaNGA ID (1)	z (2)	Class. BPT (3)	Class. WHAN (4)	R_{50} [arcsec] (5)	$\log M_* [M_{\odot}]$ (6)	$\log M_{\text{HI}} [M_{\odot}]$ (7)
10215-3703	0.0320	LIN	RG	3.2158	10.1102	-
10498-6104	0.0507	LIN	RG	3.0719	10.2670	-
10504-3703	0.0230	LIN	RG	3.6443	10.0380	-
10510-6103	0.0195	LIN	wAGN	12.2742	10.6460	-

Notes. MaNGA ID (1) is assigned following the convention "[PLATE]-[IFUDESIGN]". Redshift (2) is directly taken from the data reduction processed files. Classifications based on the BPT diagrams (3) and WHAN diagrams (4) are obtained using non-corrected from reddening emission line fluxes. The R_{50} petrossian isophote (5) and the stellar (6) and HI (7) masses are taken from the NASA-Sloan Atlas (NSA) catalogue^a. The complete version of this table is available at the CDS.

^a <https://www.sdss4.org/dr17/manga/manga-target-selection/nsa/>.

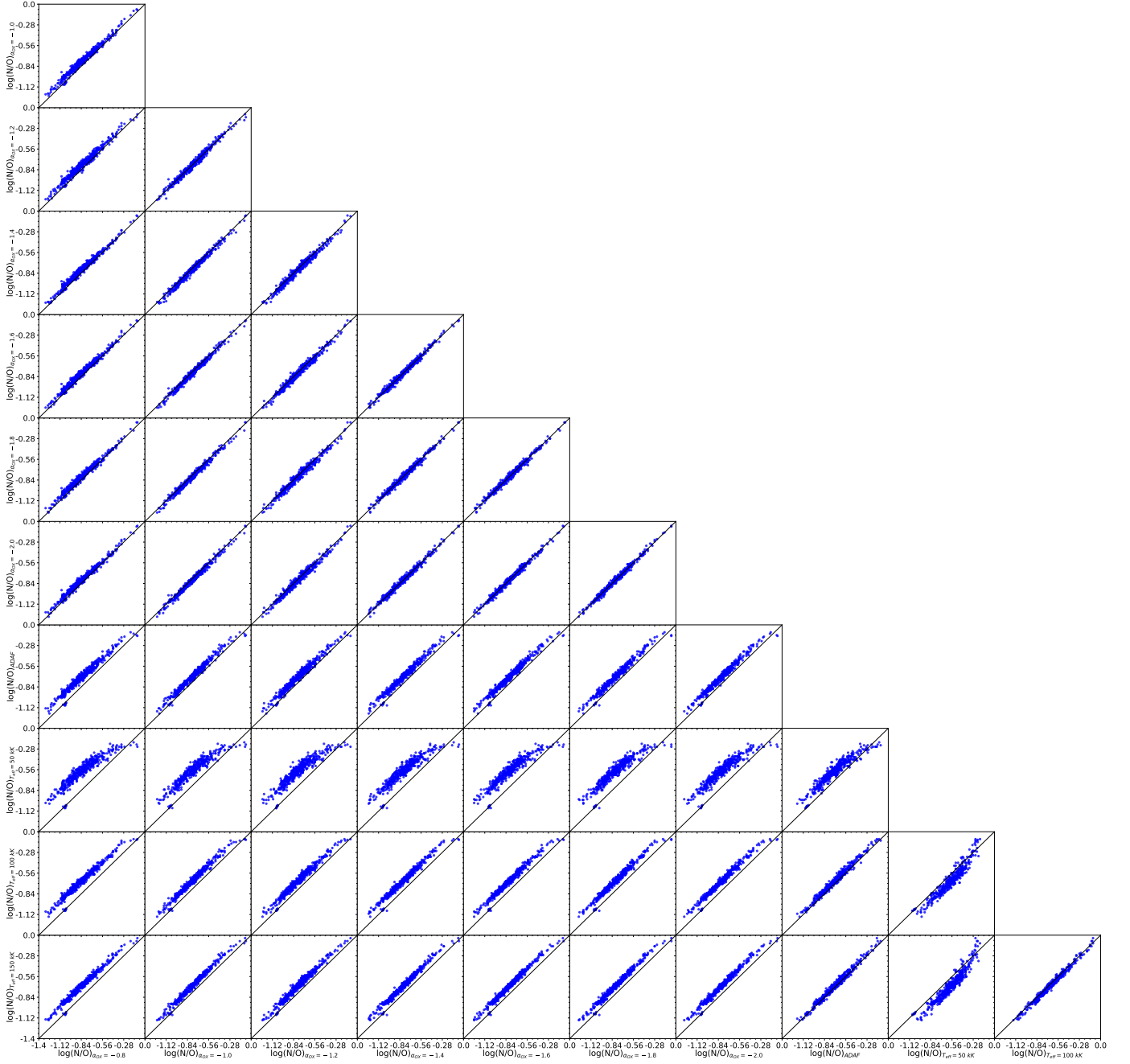


Fig. A.2. Same as Fig. A.1 but for the nitrogen-to-oxygen abundance ratio.

Table B.2. Optical spectroscopic information for our sample of LINER-like galaxies.

MaNGA ID (1)	$W_{H\alpha}$ [Å] (2)	$c(H\beta)$ (3)	[O II] λ 3727, 3729 (4)	...	[S II] λ 6717 (9)	[S II] λ 6731 (10)
10215-3703	2.74	0.1197±0.0871	3.146±0.283	...	1.407±0.144	0.865±0.100
10498-6104	2.5	0.4298±0.1100	2.844±0.357	...	1.028±0.133	0.761±0.108
10504-3703	2.18	-	2.858±0.327	...	0.985±0.154	0.943±0.153
10510-6103	3.87	1.4050±0.1157	14.617±1.595	...	1.458±0.183	1.529±0.193

Notes. Column (1): MaNGA ID. Column (2): equivalent width of $H\alpha$. Column (3): extinction coefficient based on Howarth (1983) extinction law. Columns (4)-(10): optical emission line ratios [O II] λ 3727, 3729, [Ne III] λ 3868 Å, [O III] λ 4959, [O III] λ 5007, [N II] λ 6548, [N II] λ 6584, and [S II] λ 6717, 6731 corrected from reddening and referred to $H\beta$. The complete version of this table is available at the CDS.

Table B.3. Estimated oxygen abundances in the nuclear region of our sample of LINER-like galaxies based on different grids of photoionization models.

MaNGA ID (1)	$12 + \log(O/H)_{AGN \alpha_{OX}=-0.8}$ (2)	$12 + \log(O/H)_{AGN \alpha_{OX}=-1.0}$ (3)	...	$12 + \log(O/H)_{pAGB T_{eff}=150kK}$ (12)
10215-3703	8.73±0.12	8.56±0.10	...	8.32±0.08
10498-6104	8.72±0.24	8.66±0.22	...	8.24±0.09
10504-3703	8.71±0.21	8.64±0.20	...	8.28±0.08
10510-6103	8.73±0.06	8.70±0.06	...	8.82±0.05

Notes. Column (1): MaNGA ID. Columns (2)-(12): oxygen abundances for each grid considered. The complete version of this table is available at the CDS.

Table B.4. Estimated nitrogen-to-oxygen abundance ratios in the nuclear region of our sample of LINER-like galaxies based on different grids of photoionization models.

MaNGA ID (1)	$\log(N/O)_{AGN \alpha_{OX}=-0.8}$ (2)	$\log(N/O)_{AGN \alpha_{OX}=-1.0}$ (3)	...	$\log(N/O)_{pAGB T_{eff}=150kK}$ (12)
10215-3703	-0.80±0.15	-0.74±0.13	...	-0.63±0.11
10498-6104	-0.67±0.11	-0.67±0.12	...	-0.55±0.10
10504-3703	-0.68±0.14	-0.64±0.10	...	-0.57±0.10
10510-6103	-1.20±0.13	-1.14±0.09	...	-1.06±0.11

Notes. Column (1): MaNGA ID. Columns (2)-(12): nitrogen-to-oxygen abundance ratios for each grid considered. The complete version of this table is available at the CDS.

Table B.5. Estimated ionization parameters in the nuclear region of our sample of LINER-like galaxies based on different grids of photoionization models.

MaNGA ID (1)	$\log(U)_{AGN \alpha_{OX}=-0.8}$ (2)	$\log(U)_{AGN \alpha_{OX}=-1.0}$ (3)	...	$\log(U)_{pAGB T_{eff}=150kK}$ (12)
10215-3703	-3.59±0.08	-3.71±0.04	...	-3.66±0.08
10498-6104	-3.46±0.08	-3.53±0.07	...	-3.50±0.07
10504-3703	-3.45±0.11	-3.53±0.12	...	-3.52±0.08
10510-6103	-3.74±0.05	-3.78±0.04	...	-3.81±0.04

Notes. Column (1): MaNGA ID. Columns (2)-(12): ionization parameters for each grid considered. The complete version of this table is available at the CDS.